THE ASTROPHYSICAL JOURNAL, 896:95 (22pp), 2020 June 20 https://doi.org/10.3847/1538-4357/ab94ac

A Comparison of X-Ray Photon Indices among the Narrow- and Broad-line Seyfert 1 Galaxies

Vineet Ojha[1], Hum Chand[1,2], Gulab Chand Dewangan[3], and Suvendu Rakshit[4]
[1] Aryabhatta Research Institute of Observational Sciences (ARIES), Manora Peak, Nainital—263001, India; vineetojhabhu@gmail.com
[2] Department of Physics and Astronomical Sciences, Central University of Himachal Pradesh (CUHP), Dharamshala-176215, India
[3] Inter-University Centre for Astronomy and Astrophysics (IUCAA), Pune—411007, India
[4] Finnish Centre for Astronomy with ESO (FINCA), University of Turku, Quantum, Vesilinnantie 5, FI-20014 University of Turku, Finland
Received 2019 October 11; revised 2020 April 22; accepted 2020 May 16; published 2020 June 17

Abstract

We present a detailed comparative systematic study using a sample of 221 narrow-line Seyfert 1 (NLSy1) galaxies in comparison to a redshift-matched sample of 154 broad-line Seyfert 1 (BLSy1) galaxies based on their observations using ROSAT and/or XMM-Newton in soft X-ray band (0.1–2.0 keV). A homogeneous analysis is carried out to estimate their soft X-ray photon indices (Γ_X^s) and its correlations with other parameters of nuclear activities such as Eddington ratios ($R_{\rm Edd}$), bolometric luminosities ($L_{\rm bol}$), black hole masses ($M_{\rm BH}$), and the widths of the broad component of Hβ lines (FWHM(Hβ)). In our analysis, we found clear evidence of the difference in the Γ_X^s and $R_{\rm Edd}$ distributions among NLSy1 and BLSy1 galaxies, with steeper Γ_X^s and higher $R_{\rm Edd}$ for the former. Such a difference also exists in the spectral index distribution in hard X-ray (Γ_X^h), based on the analysis of 53 NLSy1 and 46 BLSy1 galaxies in the 2–10 keV energy band. The difference in $R_{\rm Edd}$ distributions does exist even after applying the average correction for the difference in the inclination angle of NLSy1 and BLSy1 galaxies. We also estimated $R_{\rm Edd}$, based on SED fitting of 34 NLSy1 and 30 BLSy1 galaxies over the 0.3–10 keV energy band, and found that results are still consistent with $R_{\rm Edd}$ estimates based on the optical bolometric luminosity. Our analysis suggests that the higher $R_{\rm Edd}$ in NLSy1 is responsible for its steeper X-ray spectral slope compared to the BLSy1, consistent with the disk-corona model as proposed for the luminous AGNs.

Unified Astronomy Thesaurus concepts: Galaxy physics (612); Active galaxies (17); Galaxy accretion disks (562); Seyfert galaxies (1447); X-ray surveys (1824); Active galactic nuclei (16)

Supporting material: machine-readable tables

1. Introduction

Narrow-line Seyfert 1 galaxies (NLSy1s) are a peculiar class of lower-luminosity active galactic nuclei (AGNs), as defined by the width of the broad component of Hβ (FWHM(Hβ)) $\lesssim$ 2000 km s^{-1}, flux ratio of $[{\rm O_{III}}]_{\lambda 5007}/{\rm H}\beta \lesssim 3$, and strong permitted optical/UV Fe II emission lines (Shuder & Osterbrock 1981; Osterbrock & Pogge 1985; Boroson & Green 1992; Grupe et al. 1999). They show steep soft X-ray spectra and rapid X-ray flux variability (Boller et al. 1996; Wang et al. 1996; Grupe et al. 1998; Leighly 1999; Komossa & Meerschweinchen 2000; Miller et al. 2000; Klimek et al. 2004). Observations suggest that NLSy1s tend to have smaller black hole masses ($M_{\rm BH}$) and higher Eddington ratios (defined as the ratio of bolometric to Eddington luminosity $R_{\rm Edd} \equiv L_{\rm bol}/L_{\rm Edd}$) compared to the broad-line AGNs (Boroson & Green 1992; Pounds et al. 1995; Sulentic et al. 2000; Boroson 2002; Collin & Kawaguchi 2004). On the other hand, Gayathri et al. (2019) reported a similarity of $R_{\rm Edd}$ and $M_{\rm BH}$ among NLSy1s and broad-line Seyfert 1 galaxies (BLSy1s) based on the accretion disk (AD) modeling of their optical spectra. Comparatively little is known about the intrinsic emission mechanisms of NLSy1s, which are responsible for their aforementioned properties. However, since the launch of the many space telescopes such as ROSAT, Chandra, XMM-Newton, and Fermi Large Area Telescope (LAT), many NLSy1s have been detected in the high-energy bands such as X-rays and γ-rays. These high-energy emissions are thought to be one of the most direct forms of nuclear activity that do play a crucial role in understanding the accretion process in the different types of AGNs.

For instance, a remarkable correlation has been found by Boller et al. (1996) and Wang et al. (1996) between the soft X-ray photon indices and the widths of the broad component of Hβ lines (FWHM(Hβ)) in the NLSy1s. This is interpreted with the variation of accretion rate in different objects (Wandel et al. 1985; Pounds et al. 1994). To test this hypothesis, Lu & Yu (1999) have compiled a sample of Seyfert 1 galaxies, QSOs, and found that the soft X-ray photon indices strongly correlate with the accretion rates. Additionally, Laor et al. (1997) have found a correlation between the soft X-ray (0.2–2.0 keV) slope and the FWHM of the Hβ emission line in a sample of 23 low-redshift quasars, suggesting that the physical parameter driving the correlation is the Eddington ratio. Many past X-ray studies of the low-luminosity AGNs (LLAGNs, comprising low-ionization nuclear emission-line regions and local Seyfert galaxies) have been carried out to explore any correlation of X-ray photon indices with other parameters of nuclear activities (see, e.g., González-Martín et al. 2006; Panessa et al. 2006; Gu & Cao 2009). For instance, Gu & Cao (2009) find a significant anticorrelation among the hard X-ray photon indices and the Eddington ratios using a sample of 55 LLAGNs, whose X-ray photon indices are collected from the literature having Chandra or XMM-Newton observations. This anticorrelation resembles the spectra produced from the advection-dominated accretion flow (ADAF) model for the X-ray binaries (XRBs) in the low state (see, e.g., Esin et al. 1997). However, it is found to be in contrast with the positive correlation reported by Risaliti et al. (2009) for the luminous AGNs. Their analysis led to an important suggestion that the spectra of LLAGNs might be produced by the Comptonization process in ADAFs, which is similar to that of XRBs but is different from that in luminous AGNs. As a result, such analysis has important implications for the physical link between the accretion efficiency in the (cold) accretion disk of AGNs and the physical status of the (hot) corona.

For the X-ray-detected NLSy1 galaxies, either their X-ray/$\gamma-$ ray emissions can be from the jets whose existence is inferred based on their high variability in short timescales (Paliya et al. 2014; Kshama et al. 2017; Ojha et al. 2019, 2020), or they could be based on the ADAF mechanism as suggested by Gu & Cao (2009) for LLAGNs. Another possibility could be the accretion-flow/hot-corona system of radiatively efficient accretion, as suggested by Maoz (2007), where thin accretion disks may persist at lower accretion rates. Additionally, it could also be from the widely accepted disk-corona model. In this model, UV soft photons from the accretion disk are Comptonized and up-scattered (inverse Comptonization) into the X-ray bands by a hot corona, existing above the accretion disk (Haardt & Maraschi 1991, 1993). To get an insight into the emissions from the central engine of NLSy1s, one possibility is to compare the distribution of its key parameters, such as $R_{\rm Edd}$, $M_{\rm BH}$, and X-ray spectral slopes, with the control sample of BLSy1s matching in the luminosity–redshift (L–z) plane. Any observational constraints based on such comparisons can be very useful to probe the above possible mechanisms. For instance, if the $R_{\rm Edd}$ of NLSy1s in comparison to BLSy1s are statistically higher, then one would expect an increase in the disk temperature, hence the production of more X-ray radiations, and at the same time, it can also increase the Compton cooling of the corona (Haardt & Maraschi 1991, 1993; Zdziarski et al. 2000; Kawaguchi et al. 2001). This can further lead to observable steepening of the X-ray power law more in NLSy1s than in BLSy1s. Therefore, for such an insight, especially about the X-ray emission mechanism, the X-ray spectral slope (in both the soft and hard X-ray energy bands) of a statistical large sample of NLSy1s, along with its control sample of BLSy1s (matching in their L–z plane), is very useful. This can also help to parameterize the cooling and heating mechanisms of the X-ray corona, along with the underlying electrons' energy distribution.

However, the main hindrance until now in the aforementioned investigations was the lack of a reasonable statistical homogeneous sample (see Brandt et al. 1997) added by a homogeneous analysis in the soft (0.1–2.0 keV) and the hard (2–10 keV) X-ray bands for the NLSy1 and BLSy1 galaxies, preferably matching in the L–z plane. This was due to a relatively small available sample size of a total of 2000 optically detected NLSy1s given by Zhou et al. (2006) based on Sloan Digital Sky Survey (SDSS) Data Release 3 (SDSS DR3; Schneider et al. 2005). In contrast, based upon a 10-fold increase in the number of AGNs as compared to the SDSS DR3 in SDSS spectroscopic Data Release 12 (SDSS DR12; Alam et al. 2015), Rakshit et al. (2017) have recently enlarged the sample of NLSy1s to a total of 11,101 objects, which is about five times larger than the number of previously known NLSy1 galaxies based on the Zhou et al. (2006) catalog. This enlarged sample can be used to carry out a systematic and homogeneous analysis of a statistical sample of NLSy1s (in both optical and X-ray). This can further be used to compare its key parameters of nuclear activities, such as $R_{\rm Edd}$, $M_{\rm BH}$, and X-ray spectral slopes, with a control sample of BLSy1s (preferably matching in their L–z plane). This analysis is also favorable to investigate whether the steepening reported in the spectral slopes of NLSy1s (albeit deduced with small sample size; see, e.g., Brandt et al. 1997) as compared to BLSy1s exists only in soft X-ray band or also extends to the hard X-ray band, which is less prone to the soft X-ray excess (Boller et al. 1996; Brandt et al. 1997; Vaughan et al. 1999; Boller et al. 2002; Czerny et al. 2003; Vignali et al. 2004).

Here we have worked toward the aforementioned goals. For this, we have selected a sample of 221 NLSy1s by cross-correlating 11,101 NLSy1s with that of the second ROSAT all-sky survey (2RXS) source catalog of Boller et al. (2016) and based on any source observation in XMM-Newton, available in the HEASARC public data archive[5] (e.g., Section 2). The corresponding control sample of 154 BLSy1s in the X-ray band, moderately matching in redshift with that of our NLSy1 (e.g., Section 2) sample, is used to carry out the comparative study of these two subclasses.

For the homogeneous X-ray analysis of the NLSy1 and BLSy1 galaxies, similar models and homogeneous methods are adopted for estimating their X-ray spectral slopes in both the soft and hard X-ray bands. In the same way, a homogeneous method is also applied to estimate the black hole masses for all the members of our samples by careful modeling of the Hβ lines using their SDSS optical spectra. This is used to investigate any statistical relationships among the X-ray photon indices of NLSy1s and BLSy1s with their other key parameters of nuclear activities, such as FWHM(Hβ), $M_{\rm BH}$, bolometric luminosities ($L_{\rm bol}$), and $R_{\rm Edd}$. This allows us to understand the X-ray emission mechanisms of NLSy1s as compared to the BLSy1s, along with the comparison of their properties with other luminous AGNs.

The paper is structured as follows. Section 2 describes the data sample and selection criteria. Section 3 describes observations and data reduction along with our analysis for X-ray data. Section 4 gives details of our spectral analysis. In Section 5, we focus on our results, while discussion and conclusion are given in Section 6. Finally, we summarize our work in Section 7. Throughout, we have used a cosmology with $\Omega_m = 0.286$, $\Omega_\lambda = 0.714$, and $H_o = 69.6$ kms^{-1} Mpc^{-1} (Bennett et al. 2014).

2. Sample Selection

For constructing our sample of NLSy1 galaxies, we used a recent catalog of NLSy1s given by Rakshit et al. (2017), in which they have compiled 11,101 NLSy1s using the SDSS DR12 database. To make a sample of X-ray-detected NLSy1s, we have cross-correlated these 11,101 NLSy1s with the 2RXS source catalog. This cross-correlation resulted in 1873 matches in the 2RXS catalog within a position offset (in source R.A. and decl.) of 30″. Similarly, we also searched for any XMM-Newton-based observations for the above sample of 11,101 NLSy1s by using the HEASARC public data archive. This resulted in a sample of 697 XMM-Newton-observed NLSy1s such that each of the NLSy1s falls within the 27.5 arcmin^2 offset from the pointing center of the parent XMM-Newton observation. Here, for any source with multiple observation IDs, the repetition is avoided by retaining only the observation with the largest observing time. We also noticed that like

[5] https://heasarc.gsfc.nasa.gov/db-perl/W3Browse/w3browse.pl

XMM-Newton, the above energy range is also covered by the Chandra telescope, but due to its much smaller effective area (e.g., $\sim$600 cm^2) as compared to XMM-Newton ($\sim$1227 cm^2), a typical increase in sample size due to the observed sources by the Chandra telescope is found to be nominal (around $\sim$10%). Therefore, we have limited our analysis only to XMM-Newton's covered sources and the ROSAT 2RXS catalog's matched sources.

Observations in ROSAT were carried out using two detectors, viz., the Position-Sensitive Proportional Counter (PSPC) and High-Resolution Imager (HRI). Furthermore, we noted that the HRI is essentially an imager with very little spectral response. Therefore, we limited our ROSAT sample only to those sources that were observed with the PSPC instrument. This filter reduces our sample of ROSAT-detected sources from 1873 to 530.

The 0.1–2.0 keV ROSAT spectrum of each source was extracted using standard XSELECT tasks of the HEASOFT software (ver. 6.25) with the appropriate circular region around the source to enhance source signal and reduce the background noise. This is found to differ for different sources depending on the number of pixels containing the maximum flux of the source (e.g., Section 3). The impact of this choice of the aperture by eye on the signal-to-noise ratio (S/N), as well as on our analysis (since for both same aperture is used), is found to be negligible in our sample. However, a very nominal enhancement in S/N is found owing to relatively less background noise in comparison to a fixed (50$''$) aperture encircling about 90% energy fraction.

To exclude sources without high-quality data, we have put a minimum S/N criterian of 10 on our sample. For computing the S/N, we have estimated $[N_{\rm src} - N_{\rm bkg}]\big/\sqrt{(N_{\rm src} + N_{\rm bkg})}$, where $N_{\rm src}$ and $N_{\rm bkg}$ refer to the total count contributed by aperture around the source and background region, respectively. Here the background region is chosen in close proximity to the source with aperture size fixed to its value as used for extracting the source count. This aperture size either could be fixed so that it encircled about 90% energy fraction or can also be optimized to enhance the S/N, as with an increase in aperture size background noise also increases. We have opted to use the latter, though the increase in S/N using it is found to be nominal in comparison to the former method (e.g., with 50$''$ fixed aperture to encircle 90% energy). We also note that the S/N computed by the $[N_{\rm src} - N_{\rm bkg}]\big/\sqrt{(N_{\rm src} + N_{\rm bkg})}$ method is consistent with that using [count rate]/[error on count rate] as returned by XSPEC (ver. 6.25) for the source "grp" file. For our ROSAT sources, we used the 0.1–2.0 keV energy range while computing the S/N using the above [count rate]/[error on count rate] method. The S/N $\geqslant$ 10 criterion was satisfied by 83 out of 530 (henceforth also referred to as 83/530) ROSAT/PSPC (0.1–2.0 keV) detected sources. For the 697 XMM-Newton-detected NLSy1s, among its three European Photon Imaging Camera (EPIC) detectors, we have limited our analysis only to the PN detector owing to its larger effective area (about 1227 cm^2 at 1 keV). Each source spectrum was extracted over the appropriate circular aperture, selected by eye around the source, in the same way as we had done for ROSAT (e.g., Section 3). The S/N $\geqslant$ 10 criterion was satisfied by 148/697 XMM-Newton/PN sources in the 0.3–2.0 keV energy band. Further, we noticed that eight sources are common between the samples of the 83 ROSAT-selected NLSy1s and the 148 XMM-Newton-selected NLSy1s. For these eight sources, we have used only XMM-Newton observations owing to its better spectral resolution and effective area (about 1227 cm^2 at 1 keV) as compared to ROSAT (about 240 cm^2 at 1 keV). This led to our final sample of 223 sources, with 75 from ROSAT and 148 from XMM-Newton for their further X-ray spectral fitting.

To make a sample of BLSy1 galaxies matching in the *L*–*z* plane with our above sample of NLSy1 galaxies, so as to carry out their comparative study (e.g., Section 1), we have used a recent compilation of Rakshit & Stalin (2017), where they have matched the above parent sample of 11,101 NLSy1 galaxies with that of BLSy1 galaxies, both derived using SDSS DR12. In their compilation, they found a sample of 5511 NLSy1 and BLSy1 galaxies, matching in the *L*–*z* plane (e.g., their Figure 1). We noticed that out of our 223 NLSy1s, 149 (57 from ROSAT and 92 from XMM-Newton) were indeed members of this 5511-NLSy1 sample for which the *L*–*z* matched sample of 5511 BLSy1s exists.

However, due to limited X-ray observations of the aforementioned samples of NLSy1 and BLSy1 galaxies in ROSAT and XMM-Newton, we found it difficult to construct their exact *L*–*z* matched sample for the X-ray analysis. Nonetheless, by restricting our search for X-ray observations of BLSy1s only to the above sample of 5511 BLSy1s, we can expect to have a close *L*–*z* match in the X-ray-detected NLSy1 and BLSy1 samples. Therefore, we have cross-correlated these 5511 BLSy1s with those of the 2RXS catalog of ROSAT and also searched for any XMM-Newton-based observations using a similar procedure to what we had adopted in the case of the NLSy1 sample. The cross-correlation match in ROSAT resulted in 1156 BLSy1s, among which 289 were covered by the PSPC instrument. Similarly, we found observations of 332 BLSy1s in XMM-Newton. Further, we also applied the S/N $\geqslant$ 10 detection criterion, as had also been used in the sample of NLSy1s (for both the ROSAT and XMM-Newton subsamples). This resulted in a sample of 157 BLSy1s, consisting of 54 sources from ROSAT and 103 from XMM-Newton. Further, we cross-correlated the 54 ROSAT BLSy1s with the 103 XMM-Newton BLSy1s, in order to check for any common sources among them, but none of the sources were found to be common.

Furthermore, it may be noted that we have used separately XMM-Newton data for the X-ray analysis of total (0.3–10 keV) and hard (2–10 keV) energy bands as well. Out of 148 NLSy1s, the S/N $\geqslant$ 10 criterion is fulfilled by 147/148 in 0.3–10.0 keV and 56/148 in 2–10 keV. For BLSy1s, all qualify in the total 0.3–10 keV energy band, but only 51/103 meet this S/N $\geqslant$ 10 criterion in the hard energy band.

Further, reduction of the samples also occurs owing to nonconvergence of the spectral fit (perhaps due to artifacts in data; see Section 4.2), which in case of NLSy1s allow us to use 139/147 in 0.3–10 keV, 146/148 in 0.1–2.0 keV, and 53/56 in 2–10 keV. Similarly, for BLSy1s we could fit the XMM-Newton sample of 97/103 in 0.3–10 keV, 100/103 in 0.1–2.0 keV, and 46/51 in 2–10 keV, as also summarized in Table 1. This led to our final samples of 221 NLSy1s (75 from ROSAT and 146 from XMM-Newton) and 154 BLSy1s (54 from ROSAT and 100 from XMM-Newton), for which we have shown the histograms of their redshift and luminosity in Figure 1. As the figure shows, these two samples of NLSy1s and BLSy1s do moderately match in redshift, having median

Table 1
Summary of the Sample Selection of NLSy1 and BLSy1 Galaxies

Telescope Used	Selected (Taken[a])					
	Soft Energy Sample		Hard Energy Sample		Total (0.3–10 keV) Energy Sample	
	NLSy1	BLSy1	NLSy1	BLSy1	NLSy1	BLSy1
ROSAT	530 (075)	289 (054)	— —	— —	— —	— —
XMM-Newton	697 (146)	332 (100)	148 (53)	103 (46)	148 (139)	103 (97)
BOTH (XMM+ROSAT)	1227 (221)	621 (154)	148 (53)	103 (46)	148 (139)	103 (97)

Note.
[a] After imposing a minimum $S/N \geqslant 10$ detection criterion (using the 0.1–2.0 keV range in ROSAT and the 0.3–10 keV range in XMM-Newton) and counting the repeated sources only once (retaining only XMM-Newton sources; e.g., Section 2), along with the exclusion of those sources that could not be fitted with the adopted models (e.g., Section 4.2).

redshifts of 0.21 and 0.26, respectively. This gives the Kolmogorov–Smirnov (K-S) test based probability of null hypothesis ($P_{\rm null}$) of ∼3%. However, the difference in luminosity is found to be much higher with median values of $\log(\lambda L_\lambda(5100\,\text{Å}))$ [erg/s/Å] of 43.67 and 44.08, respectively, and $P_{\rm null} = 2.43 \times 10^{-8}$.

3. Observations and Data Reduction

The X-ray data of our NLSy1 and BLSy1 galaxies were based on observations taken either with ROSAT/PSPC or with XMM-Newton/EPIC telescopes. The ROSAT 0.1–2.0 keV spectrum of each NLSy1 and BLSy1 was extracted using the appropriate circular region around the source (see, e.g., third paragraph of Section 2). However, while extracting the corresponding background spectrum for a given source, we had ensured that its circular aperture is of the same size as taken for the source and is also in the vicinity of the source, free from any contamination from the other X-ray objects.

The standard XMM-Newton Science Analysis System (SAS) software package (ver. 16.1.0) was used in data reduction of the PN detector of XMM-Newton/EPIC with updated calibration files. The EPCHAIN task was used on EPIC "Observation Data Files" for the preliminary processing. Calibrated and concatenated event lists were extracted using the EVSELECT task of SAS. We checked each source's data set for the high background proton flares by making its light curve in the 10–12 keV energy range, which is used to make the good time interval (*gti*) file. Furthermore, pileup was also checked for each source's data set using the EPATPLOT task of SAS, with the appropriate circular region around the source, depending on the number of pixels containing the maximum flux of the source. If found, then that was removed by taking only the annulus region around the source for that data set. The SAS task ESPECGET was used to generate background and background-corrected source spectra. Further, it may be noted that we have used the χ^2 minimization technique in our analysis, for which the essential criterion is that the data points included in this technique should be independent. Hence, while grouping our spectral data of XMM-Newton, we have taken care of this point and grouped each spectrum with a minimum of 20 counts subject to a condition that there should not be more than 4 bins per spectral resolution. This was done using the special task SPECGROUP of SAS software.

4. Analysis

4.1. Black Hole Mass and Eddington Ratio Measurement

To estimate the $M_{\rm BH}$ in a homogeneous way as pointed out in Section 1, we have opted to use the single-epoch virial method, with improved virial empirical relation given by Vestergaard & Peterson (2006) as

$$\log M_{\rm BH} = \log\left[\left(\frac{FWHM\,(H\beta)}{1000\ {\rm km\ s^{-1}}}\right)^2\right] + (6.91 \pm 0.02) + \log\left(\frac{\lambda L_\lambda(5100\ \text{Å})}{10^{44}\ {\rm erg\ s^{-1}}}\right)^{0.50\pm0.06}, \quad (1)$$

where $L_\lambda(5100\ \text{Å})$ is the monochromatic power-law continuum luminosity at 5100 Å and FWHM(Hβ) is the width of the broad component of the Hβ line. We have taken both these parameters from the parent catalog of NLSy1s given by Rakshit et al. (2017). The procedure to obtain these parameters for BLSy1s was also similar to that used in NLSy1s, as outlined in Rakshit et al. (2017). In brief, in their method they have first carried out a simultaneous fit of an AGN power-law continuum and host galaxy contribution, by masking the AGN emission lines. In the second step, a simultaneous fit on the host-galaxy-subtracted spectrum is carried out to optimize the best-fit Gaussian profiles for the broad and narrow components of Hβ lines coming from the AGN broad- and narrow-line regions, respectively, along with the underneath local continuum and blends of Fe II emissions (see, e.g., Rakshit et al. 2017).

Finally, for the estimations of the Eddington ratio, we have taken $L_{\rm bol} = 9.8 \times \lambda L_\lambda(5100\ \text{Å})$ (McLure & Dunlop 2004) and $L_{\rm Edd} = 1.45 \times 10^{38}\ (M_{\rm BH}/M_\odot)\ {\rm erg\ s^{-1}}$, assuming a mixture of hydrogen and helium so that the mean molecular weight is $\mu = 1.15$. The values of $\log(M_{\rm BH})$ and $\log(R_{\rm Edd})$ along with Γ^h_X, Γ^s_X, and Γ^T_X for each NLSy1 and BLSy1 galaxy are given in Columns (6), (7), (8), (11), and (14) of Tables 3 and 4, respectively.

4.2. X-Ray Spectral Analysis

For the spectral analysis of 75 NLSy1 and 54 BLSy1 ROSAT-detected galaxies, we have used XSPEC version 12.10.1 (Arnaud 1996; Dorman & Arnaud 2001) tasks of HEASOFT. The response matrices files (RMFs) required for

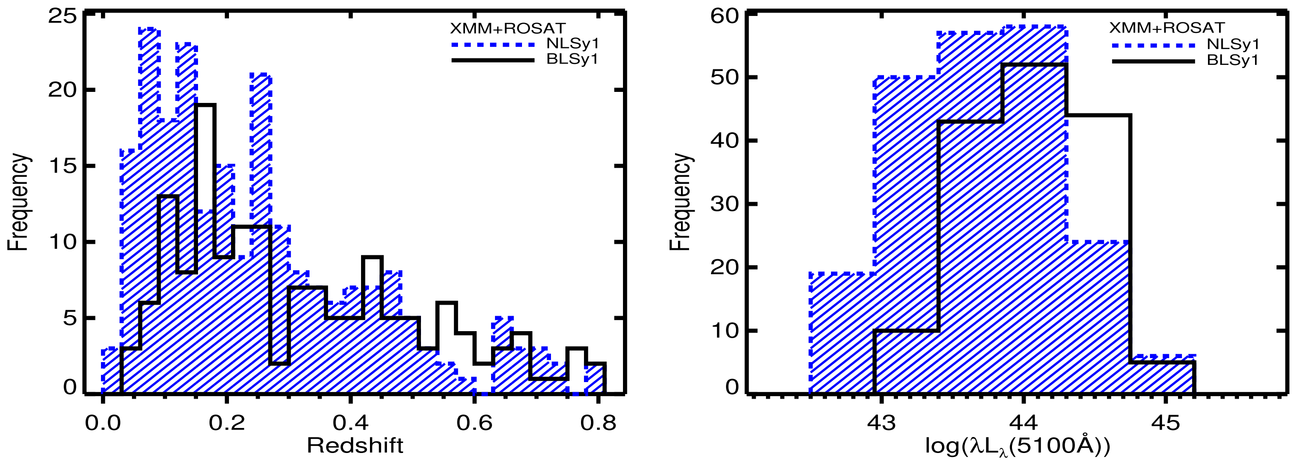

Figure 1. Distribution of emission redshifts (left) and λL_λ(5100 Å) (right) for our XMM-Newton- and ROSAT-detected combined samples of 221 NLSy1s (blue filled histogram) and 154 BLSy1s (black open histogram).

Table 2
Summary of the Best-fit Model Used for the Spectral Fitting of NLSy1 and BLSy1 Galaxies

Parameter	Model	NLSy1	BLSy1
		0.1–2.0 keV	
Γ_X^s	*tbabs* × *ztbabs* × *zpowerlw*	74 (ROSAT) 143 (XMM-Newton)	54 (ROSAT) 98 (XMM-Newton)
	tbabs × *ztbabs* × (*zpowerlw*+*zbbody*)	01 (ROSAT) 003 (XMM-Newton)	02 (XMM-Newton)
		2–10 keV	
Γ_X^h	*tbabs* × *ztbabs* × *zpowerlw*	052 (XMM-Newton)	44 (XMM-Newton)
	tbabs × *ztbabs* × (*zpowerlw*+*zbbody*+Gauss)	001 (XMM-Newton)	02 (XMM-Newton)
		0.3–10 keV	
Γ_X^T	*tbabs* × *ztbabs* × *zpowerlw*	082 (XMM-Newton)	68 (XMM-Newton)
	tbabs × *ztbabs* × (*zpowerlw*+*zbbody*)	045 (XMM-Newton)	26 (XMM-Newton)
	tbabs × *ztbabs* × (*zpowerlw*+*zbbody*+Gauss)	009 (XMM-Newton)	02 (XMM-Newton)
	tbabs × *ztbabs* × *zbknpower*	002 (XMM-Newton)	01 (XMM-Newton)
	tbabs × *ztbabs* × (*zbknpower*+*zbbody*)	001 (XMM-Newton)	——— ———

the spectral fitting were obtained from the latest calibration database available publicly on the HEASARC calibration database,[6] and the ancillary response files (ARFs) were generated with the PCARF task of HEASOFT. The extracted spectrum (e.g., Section 3) of each NLSy1 and BLSy1 was grouped with a minimum of 20 counts bin^{-1} using the GRPPHA routine of the XSELECT task, which permitted us to use χ^2 minimization for spectral fitting. To obtain the soft X-ray (0.1–2.0 keV) photon indices (hereafter Γ_X^s), we have used the physically motivated model consisting of a basic power law and the double neutral absorption (i.e., *tbabs* × *ztbabs* × *zpowerlw*) in XSPEC software to the spectral data in the observed frame energy range of 0.1–2.0 keV. Special care was taken to properly fit the absorption of soft X-rays during the fitting of NLSy1 and BLSy1 galaxies. During the fitting, the redshift of the source was kept fixed to its precise value known from its optical spectrum, and also Galactic hydrogen column density in the direction of the source was kept fixed based on the value given by Dickey & Lockman (1990). However, the normalization, host galaxy absorption, intrinsic absorption, and Γ_X^s of the source were the free parameters of the fit. In one of our NLSy1 galaxies, viz., J162901.20+400758.8, we noted soft X-ray excess below 0.5 keV. For fitting this source, we added a blackbody component to our basic model (i.e., *tbabs* × *ztbabs* × (*zpowerlw*+*zbbody*)). In summary, we could estimate, using ROSAT data in the 0.1–2.0 keV range, the Γ_X^s of 75 NLSy1 and 54 BLSy1 galaxies, as listed in Tables 3 and 4 (see Columns (11)–(13)), respectively.

For spectral analysis of the XMM-Newton/EPIC-PN sample, we have used physically motivated models as had been employed above for the ROSAT/PSPC sample. Our model fittings converged well to estimate soft X-ray (0.3–2.0 keV) photon indices for the 146/148 NLSy1s and 100/103 BLSy1s, and for the hard X-ray (2–10 keV) photon indices (hereafter Γ_X^h) in 53/56 NLSy1s and 46/51 BLSy1s. Among them, 51 NLSy1s and 44 BLSy1s were fitted in both hard and soft energy bands of XMM-Newton, while 2 NLSy1s and 2 BLSy1s were only fitted in the hard X-ray energy band. We also noticed the soft X-ray excesses in 3 NLSy1s and 2 BLSy1s and fitted them by adding a blackbody component to our basic model. However, one NLSy1 galaxy (viz., J105128.32+335851.6) and 2 BLSy1 galaxies (viz., J125553.04+272403.6 and J161745.6+060350.4) also showed an emission-line feature. Therefore, to fit these sources, we had added the blackbody and Gaussian components to our basic model, viz., *tbabs* × *ztbabs* × (*zpowerlw*+*zbbody*+Gauss). A summary of these best-fit models is given in Table 2.

6 https://heasarc.gsfc.nasa.gov/docs/heasarc/caldb/

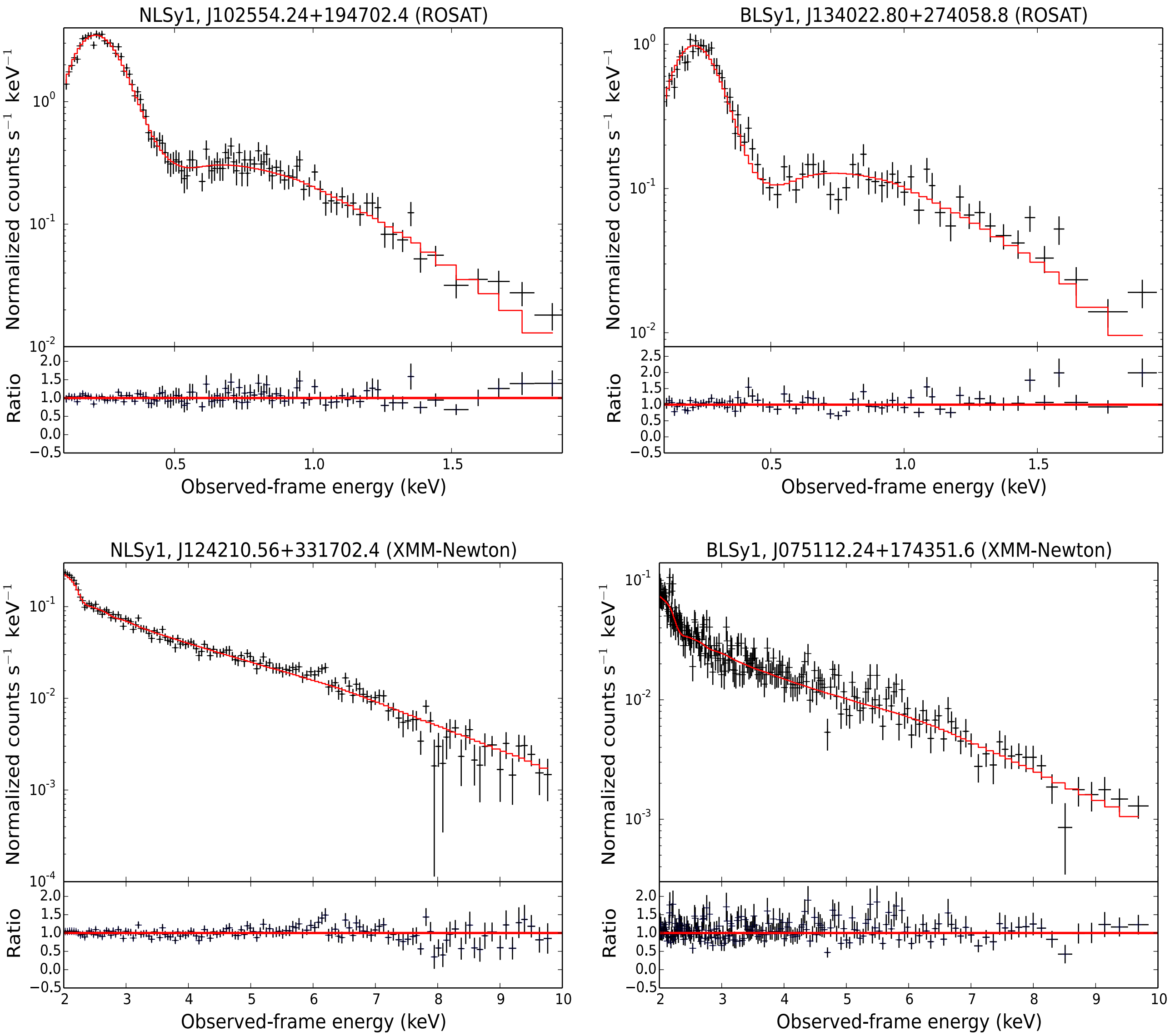

Figure 2. Top: representative ROSAT soft (0.1–2.0 keV)/PSPC data and best-fit folded models for the NLSy1 galaxy, J102554.24+194702.4 (top left panel), and the BLSy1 galaxy, J134022.80+274058.8 (top right panel). In each case, our fit was carried out using power-law and double neutral absorption models. Bottom: same as the top panels, but for the XMM-Newton hard (2–10 keV)/PN data of the NLSy1 galaxy, J124210.56+331702.4 (bottom left panel), and the BLSy1 galaxy, J075112.24+174351.6 (bottom right panel).

Representative data and best-fit folded models for one member of the NLSy1 and BLSy1 samples, each in ROSAT and XMM-Newton, are shown in the top and bottom panels of Figure 2, respectively. The typical range of the X-ray photon index varies for our samples of NLSy1 and BLSy1 galaxies in the soft energy band from 1.1–4.4 and 1.3–3.6, respectively, while in the hard energy band it varies from 1.2–2.6 and 1.2–2.7, respectively.

In summary, based on our combined sample of 223 NLSy1s (75 from ROSAT and 148 from XMM-Newton), we got Γ_X^s measurements for the 221 NLSy1s (75 from ROSAT and 146 from XMM-Newton) as listed in Table 3. Similarly, out of the sample of 156 BLSy1s (54 from ROSAT and 103 from XMM-Newton), we got Γ_X^s for 154 BLSy1s (54 from ROSAT and 100 from XMM-Newton) as listed in Table 4. The histograms and cumulative probability distribution functions (CPDFs) of Γ_X^s for the samples of 221 NLSy1 and 154 BLSy1 galaxies, along with their combined sample (hereafter [NLSy1+BLSy1]), are shown in the top panels of Figure 3. However, for the Γ_X^h measurements, we could use only 53 NLSy1 and 46 BLSy1 galaxies based on their XMM-Newton subsamples of 56 NLSy1 and 51 BLSy1 galaxies, as listed in Tables 3 and 4, respectively. The histograms and CPDFs of Γ_X^h are shown in the top panels of Figure 4.

4.3. X-Ray Spectral Analysis in 0.3–10 keV Energy Range

The spectral coverage of the XMM-Newton data also allows us to estimate the 0.3–10 keV photon indices (hereafter Γ_X^T). This is also useful to compare the Γ_X^T distribution with the Γ_X^s and Γ_X^h distributions, for both NLSy1 and BLSy1 galaxies. Our fittings in the 0.3–10 keV range could converge for 82/146 NLSy1s and 68/100 BLSy1s with our basic model, i.e., *tbabs* × *ztbabs* × *(zpowerlw)*. However, in the case of 45 NLSy1 and 26 BLSy1 galaxies, we had to add a blackbody component to our basic model, i.e., *tbabs* × *ztbabs* × (*zpowerlw*+*zbbody*). An additional Gaussian emission component was required for the fittings of 8 NLSy1 and 2 BLSy1 galaxies, i.e., *tbabs* × *ztbabs* × *(zpowerlw +zbbody+Gauss)*. For 2 NLSy1s (viz., J150506.48+032631.2,

Table 3
Details of Our Spectral Analysis of 221 NLSy1 Galaxies in the Soft Energy Band (0.1–2.0 keV), Including the 53 and 139 NLSy1s Analyzed Also in the Hard (2–10 keV) and Total (0.3–10 keV) Energy Bands, Respectively

Source Name	RA (deg)	DEC (deg)	z_{em}	S/N (0.3–10 keV)	log $M_{\rm BH}$	log $R_{\rm Edd}$	Γ_X^h (2–10 keV)	$\delta\Gamma_X^{h-}$ (2–10 keV)	$\delta\Gamma_X^{h+}$ (2–10 keV)	Γ_X^s (0.1–2.0 keV)	$\delta\Gamma_X^{s-}$ (0.1–2.0 keV)	$\delta\Gamma_X^{s+}$ (0.1–2.0 keV)	Γ_X^T (0.3–10 keV)	$\delta\Gamma_X^{T-}$ (0.3–10 keV)	$\delta\Gamma_X^{T+}$ (0.3–10 keV)	log(λL_λ) (5100 Å) erg s^{-1}	FWHM (Hβ) (km s^{-1})	$\delta(FWHM(H\beta))$ (km s^{-1})	Aperture Used (arsec)	Telescope Used
(1)	(2)	(3)	(4)	(5)	(6)	(7)	(8)	(9)	(10)	(11)	(12)	(13)	(14)	(15)	(16)	(17)	(18)	(19)	(20)	(21)
J010712.00 +140845.6	016.800	14.146	0.0767	054.0	6.0221	−0.6422	2.0618	−0.2783	0.5270	2.5856	−0.1670	0.2440	2.4017	−0.0501	0.0797	42.55	829	29	12.59	XMM
J014644.88 −004044.4	026.687	−00.679	0.0824	030.2	6.7026	−0.6527	—	—	—	2.9201	−0.2971	0.3178	—	—	—	43.22	1234	20	57.25	ROSAT
J081442.00 +212916.8	123.675	21.488	0.1626	175.6	7.3140	−0.4641	2.0722	−0.0711	0.1415	2.7822	−0.0454	0.0715	2.8400	−0.0875	0.1012	44.02	1574	22	35.87	XMM
.....	.....	.....	.....	.....	.....	.....	.....	.....	.....	.....	.....	.....	.....	.....	.....	.....	.....	.....	.....	.....

(This table is available in its entirety in machine-readable form.)

Table 4
Details of Our Spectral Analysis of 154 BLSy1 Galaxies in the Soft Energy Band (0.1–2.0 keV), Including the 46 and 97 BLSy1s Analyzed Also in the Hard (2–10 keV) and Total (0.3–10 keV) Energy Bands, Respectively

Source Name	R.A. (deg)	Decl. (deg)	z_{em}	S/N	log $M_{\rm BH}$	log $R_{\rm Edd}$	Γ_X^h	$\delta\Gamma_X^{h-}$ (2–10 keV)	$\delta\Gamma_X^{h+}$	Γ_X^s	$\delta\Gamma_X^{s-}$ (0.1–2.0 keV)	$\delta\Gamma_X^{s+}$	Γ_X^T	$\delta\Gamma_X^{T-}$ (0.3–10 keV)	$\delta\Gamma_X^{T+}$	log(λL_λ) (5100 Å) erg s^{-1}	FWHM (Hβ) (km s^{-1})	δ(FWHM($H\beta$)) (km s^{-1})	Aperture Used (arcsec)	Telescope Used
(1)	(2)	(3)	(4)	(5)	(6)	(7)	(8)	(9)	(10)	(11)	(12)	(13)	(14)	(15)	(16)	(17)	(18)	(19)	(20)	(21)
J002113.20 −020115.6	005.305	−02.021	0.7621	024.6	8.8620	−1.5821	—	—	—	1.8349	−0.2342	0.4626	1.9144	−0.1726	0.2121	44.45	7303	733	16.45	XMM
J044759.52 −043231.2	071.998	−04.542	0.2569	016.2	8.5913	−1.6014	—	—	—	2.7118	−0.1975	0.3120	—	—	—	44.16	6318	131	93.79	ROSAT
J075112.24 +174351.6	117.801	17.731	0.1861	169.6	7.9220	−1.1421	1.7954	−0.0854	0.0580	2.2096	−0.0355	0.0711	2.1931	−0.0185	0.0595	43.95	3299	54	22.77	XMM
.....	.....	.....	.....	.....		.....	.....	.....	.....	.....	.....	.....	.....	.....	.....	.....	.....	.....	.....	.....

(This table is available in its entirety in machine-readable form.)

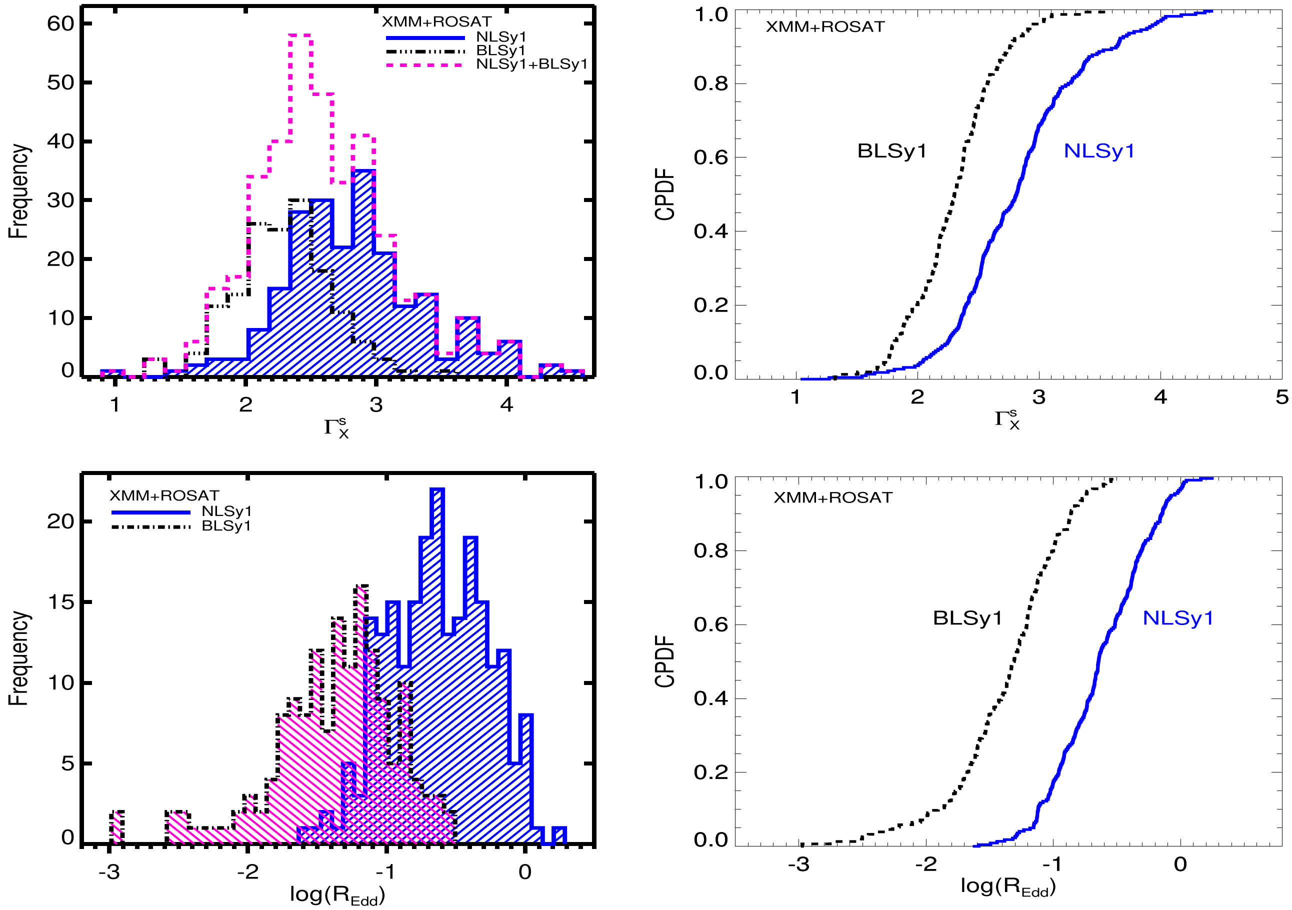

Figure 3. Top: distribution of 0.1–2.0 keV soft X-ray photon indices (left) and its CPDF (right) for our combined ROSAT and XMM-Newton soft X-ray (0.1–2.0 keV) detected samples of 221 NLSy1s (blue filled) and 154 BLSy1s (black dashed with dotted line), along with the joint [NLSy1+BLSy1] sample of 375 galaxies (pink, dashed). Bottom: same as the top panels, but for the Eddington ratio distribution (left, with blue filled for NLSy1s and pink filled for BLSy1s) and its CPDF (right), except for the joint [NLSy1+BLSy1] sample of 375 galaxies.

J151312.48+001937.2) and 1 BLSy1 (viz., J135435.76+180516.8), it was found that they cannot be fitted with a single power law; therefore, they were accounted for by a broken power-law model i.e., *tbabs* × *ztbabs* × (*zbknpower*). For one NLSy1, viz., J12410.56+331702.4, a similar feature with additional soft X-ray excess was accommodated by the inclusion of blackbody emission, e.g., as *tbabs* × *ztbabs* × (*zbknpower*+ *zbbody*). The above combination of models, as also summarized in Table 2, has allowed us to estimate $\Gamma_X^{\rm T}$ of 139/148 NLSy1 and 97/100 BLSy1 galaxies, whose distributions are shown in Figure 5. From these distributions, it can be seen that the typical range of $\Gamma_X^{\rm T}$ varies for our subsamples of NLSy1 and BLSy1 galaxies in the total energy band from 1.4–4.3 to 1.4–3.4, respectively, which is consistent with the ranges $\Gamma_X^{\rm s}$ and $\Gamma_X^{\rm h}$ (see, e.g., Section 4.2).

4.4. X-Ray Spectral Analysis in 0.3–10 keV Energy Range Using the AGNSED Model

Another physically motivated model consisting of the spectral energy distribution of the AGN (hereafter AGNSED, or "agnsed"; Kubota & Done 2018) and the Galactic absorption (i.e., *tbabs* × *agnsed*) can also be employed using XSPEC on the XMM-Newton spectra in the 0.3–10 keV energy range. Here we have limited ourselves only to those 53 NLSy1 and 46 BLSy1 XMM-Newton sources, for which their hard energy data have enabled us (due to sufficient S/N) to estimate their Γ_X^h as well (e.g., Section 4.2). Special care was also taken to properly fit the absorption of soft X-rays, by fixing the Galactic hydrogen column density to its value given by Dickey & Lockman (1990). During the fitting, black hole mass, redshift, and comoving (proper) distance of the source were kept fixed to their precise value known from the optical spectra. We also kept fix the black hole spin, inclination angle i (for the warm Comptonizing component and the outer disk), electron temperature (for the hot Comptonization component), reprocessing, and normalization parameters to 0.5, 30°, 100 keV, 0, and 1, respectively. However, the other parameters of this model, viz., Eddington ratio ($R_{\rm Edd}^{\rm SED} = \dot{m}$), electron temperature for the warm Comptonization component ($kT_e^{\rm warm}$), hot photon index ($\Gamma_X^{\rm hot}$), warm photon index ($\Gamma_X^{\rm warm}$), outer radius of the hot Comptonization component, and outer radius of the warm Comptonization component, were kept free.

In three NLSy1 and two BLSy1 galaxies, we noted a soft X-ray feature or warm absorption below 2 keV. To carry out the fitting of these five sources, we considered a warm absorber model, namely, *zxipcf* in addition to the above model (i.e., *tbabs* × *zxipcf* × *agnsed*). The above combination of models allowed us to estimate $\Gamma_X^{\rm hot}$ and $R_{\rm Edd}^{\rm SED}$ of 34 NLSy1 and 30 BLSy1 galaxies, whose distributions are shown in Figure 6. However, the fit of the remaining 19 NLSy1 (out of a total of 53) and 16 BLSy1 (out of a total of 46) galaxies did not converge with either of the above models owing to either their

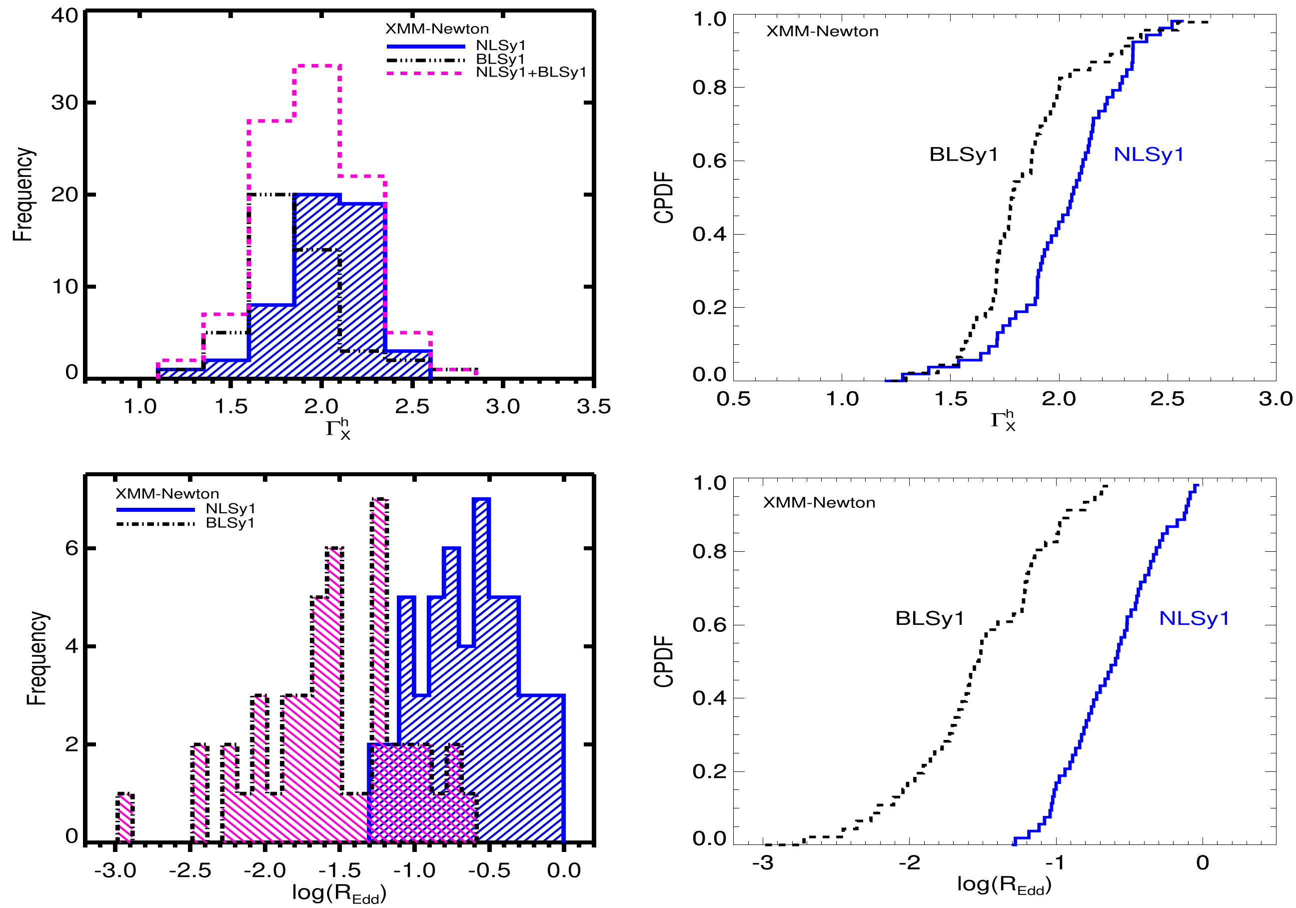

Figure 4. Same as Figure 3, but using the XMM-Newton hard X-ray (2–10 keV) detected subsamples of 53 NLSy1 and 46 BLSy1 galaxies.

bad data coverage up to 10 keV or nonconvergence of their fit parameters.

5. Results

5.1. Comparison of Γ_X and R_{Edd} among the Samples of BLSy1 and NLSy1 Galaxies

We used a sample of 221 NLSy1s to compare its physical parameters with 154 BLSy1s (see, e.g., Table 1, Section 2) moderately matching in the redshift plane (see, e.g., Figure 1). The histograms of our homogeneous analysis (e.g., Section 4.2) of 0.1–2.0 keV photon indices for both samples are shown in the top left panel of Figure 3. As can be seen from these histogram plots, there is a clear difference in the photon index distributions, with median values of 2.81 and 2.30 for the samples of NLSy1 and BLSy1 galaxies, respectively, with the former being systematically steeper. This is also evident from the CPDF plots of Γ_X^s as shown in the top right panel of Figure 3. To quantify this difference statistically, we have carried out the K-S test giving the probability of the null hypothesis (i.e., two distributions are similar) as $P_{\rm null} = 4.02 \times 10^{-19}$, suggesting a clear significant difference. Similarly, we have also plotted distributions of $R_{\rm Edd}$ for both NLSy1 and BLSy1 galaxies in the bottom panels of Figure 3. As can be seen from its histograms (bottom left panel) and CPDFs (bottom right panel), $R_{\rm Edd}$ of the sample of 221 NLSy1s is systematically higher as compared to the sample of 154 BLSy1s, with the median values of 0.23 and 0.05, respectively, resulting in a K-S test based $P_{\rm null}$ of 2.66×10^{-35}.

Furthermore, we also did the above comparison in the hard energy band (2–10 keV) using the Γ_X^h estimated for the subsamples of 53 NLSy1 and 46 BLSy1 galaxies with their distributions as shown in the top left panel of Figure 4. The Γ_X^h for the subsamples of NLSy1 and BLSy1 galaxies have median values of 2.06 and 1.78, respectively, and a K-S test based $P_{\rm null}$ of 5.13×10^{-5}, suggesting a smaller difference in their photon indices in comparison to the difference found in the soft energy band.

Additionally, we also carried out a similar comparison in the total energy band (0.3–10 keV) using the Γ_X^T of 139 NLSy1 and 97 BLSy1 galaxies with their distributions as shown in the top left panel of Figure 5. The median values of Γ_X^T for the subsamples of NLSy1 and BLSy1 galaxies are found to be 2.53 and 2.13, respectively, resulting in a K-S test based $P_{\rm null}$ of 4.50×10^{-9}. This still suggests a significant difference in their photon indices, though it is smaller than the difference found in the soft energy band.

Furthermore, quantification of any such physical differences among NLSy1 and BLSy1 galaxies can also be obtained based on the correlations of spectral indices (in the soft hard and total 0.3–10 keV X-ray energy bands) with the other parameters of nuclear activities of AGNs such as $R_{\rm Edd}$, $L_{\rm bol}$, $M_{\rm BH}$, and FWHM(Hβ), as we discuss in the next subsection.

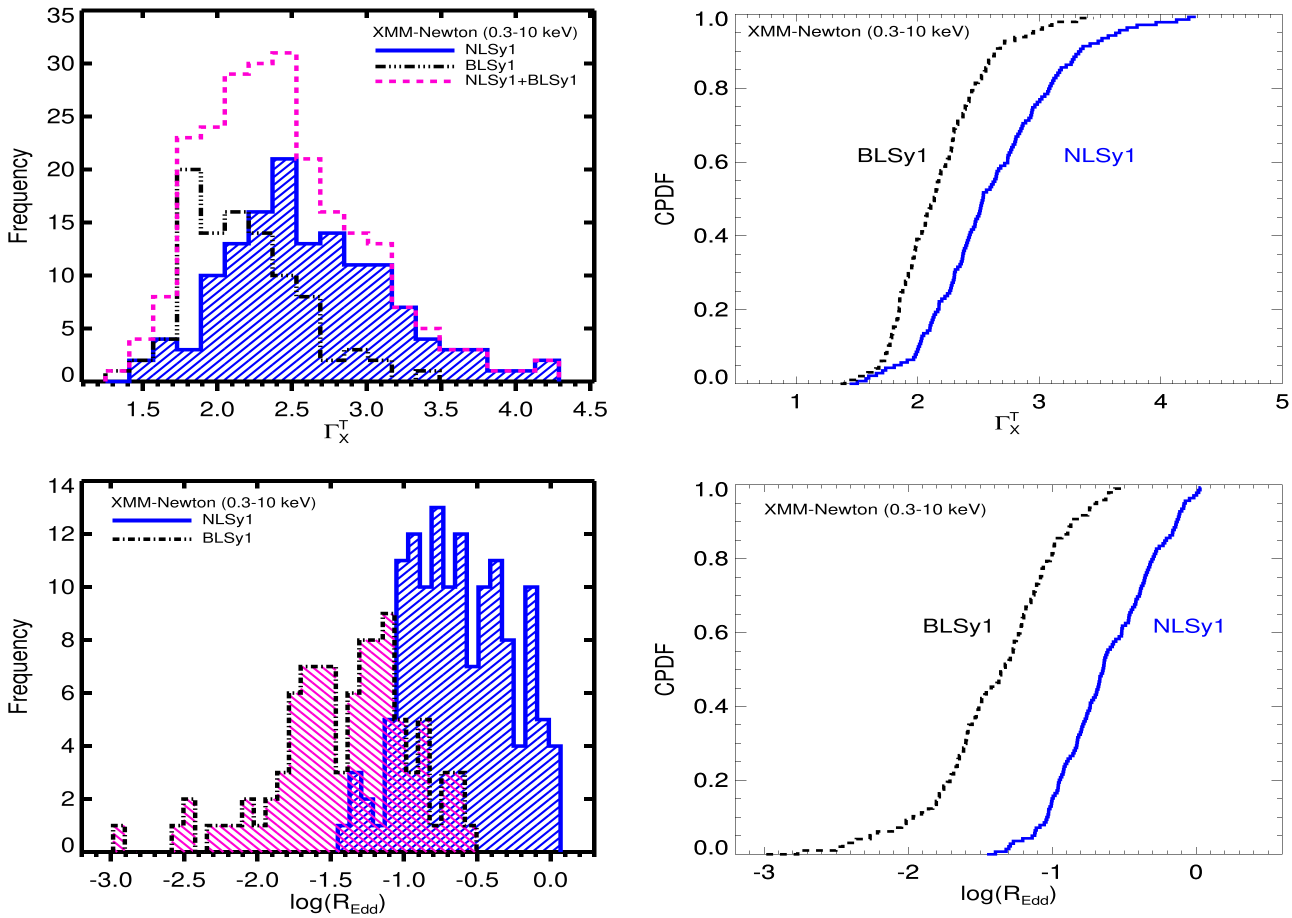

Figure 5. Same as Figure 3, but using the XMM-Newton X-ray (0.3–10 keV) detected subsamples of 139 NLSy1 and 97 BLSy1 galaxies.

5.2. Comparison of Γ_X Correlations with AGN Parameters among the Samples of NLSy1 and BLSy1 Galaxies

Results based on our correlation analysis for the samples of 221 NLSy1s, 154 BLSy1s, and their combined sample (i.e., 375 [NLSy1+BLSy1]) are shown in Figure 7. This figure shows the plots of $R_{\rm Edd}$, $L_{\rm bol}$, $M_{\rm BH}$, and FWHM(Hβ) versus Γ_X^s for NLSy1, BLSy1, and [NLSy1+BLSy1] galaxies in the left, middle, and right panels, respectively. The statistical quantifications of correlations of these parameters with Γ_X^s are summarized in Table 5. As can be seen from the top panels of Figure 7, the positive correlations between Γ_X^s and $\log(R_{\rm Edd})$ are quite apparent for the samples of NLSy1 (top left panel), BLSy1 (top middle panel), and [NLSy1+BLSy1] (top right panel) galaxies, respectively. We have also quantified these correlations with the fitting function of the form $y = mx + c$ by the standard χ^2-minimization method, which yields the relations, for the sample of NLSy1s as

$$\Gamma_X^s = (0.67 \pm 0.04)\log(R_{\rm Edd}) + (3.27 \pm 0.02), \quad (2)$$

for the sample of BLSy1s as

$$\Gamma_X^s = (0.37 \pm 0.03)\log(R_{\rm Edd}) + (2.79 \pm 0.04) \quad (3)$$

and for the joint sample of NLSy1 and BLSy1 galaxies as

$$\Gamma_X^s = (0.62 \pm 0.02)\log(R_{\rm Edd}) + (3.19 \pm 0.02) \quad (4)$$

as shown by the solid red line in the plots of $\Gamma_X^s - \log(R_{\rm Edd})$ in the top panels of Figure 7. This very good correlation is also supported based on their Spearman's rank correlation coefficient (ρ) of 0.44, 0.41, and 0.62 with the probability of null correlation ($P_{\rm null}$) of 1.28×10^{-11}, 1.71×10^{-7}, and 1.16×10^{-40} for the samples of NLSy1, BLSy1, and [NLSy1+BLSy1] galaxies, respectively. We note here that the correlation coefficients found for the samples of NLSy1 and BLSy1 galaxies are almost similar; however, the difference is significant in the slopes of their $\Gamma_X^s - \log(R_{\rm Edd})$ linear fit, with $m = 0.67 \pm 0.04$ and 0.37 ± 0.03, respectively. Our above correlations between Γ_X^s and $\log(R_{\rm Edd})$ give a hint that $\Gamma_X^s \propto L_{\rm bol}/L_{\rm Edd}$, which implies that $\Gamma_X^s \propto L_{\rm bol}$ and $\Gamma_X^s \propto L_{\rm Edd}^{-1}$. Since we know that $L_{\rm Edd} \propto M_{\rm BH}$ and $M_{\rm BH} \propto (FWHM(H\beta))^2$, therefore a very good $\Gamma_X^s - \log(R_{\rm Edd})$ correlation can be due to intrinsic $\Gamma_X^s - \log(L_{\rm bol})$ and $\Gamma_X^s - \log(M_{\rm BH}^{-1})$ correlations or due to both these correlations. We tested these possibilities in the samples of NLSy1, BLSy1, and [NLSy1+BLSy1] galaxies. We find a significant $\Gamma_X^s - \log(L_{\rm bol})$ correlation for the sample of NLSy1s with $\rho = 0.36$, $P_{\rm null} = 4.10 \times 10^{-8}$. The corresponding correlations are found to be nonsignificant for the samples of BLSy1 (with $\rho = 0.08$ and $P_{\rm null} = 0.30$) and [NLSy1+BLSy1] galaxies (with $\rho = 0.04$ and $P_{\rm null} = 0.47$). However, for the $\Gamma_X^s - \log(M_{\rm BH})$, we found a good anticorrelation in the joint sample of NLSy1 and BLSy1 galaxies (with $\rho = -0.40$ and $P_{\rm null} = 1.73 \times 10^{-15}$), though it was found to be nonsignificant when the samples of NLSy1 and BLSy1 galaxies were considered separately.

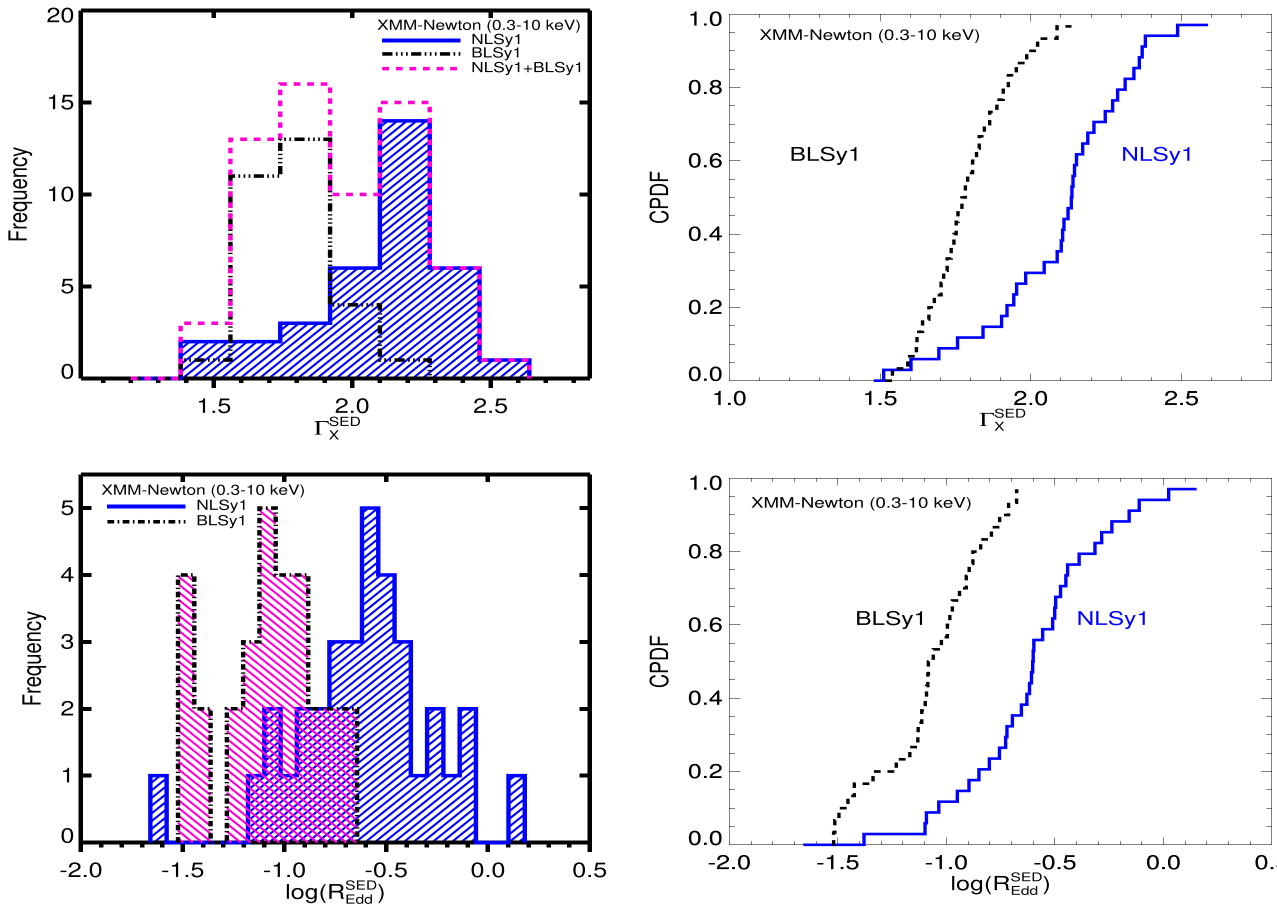

Figure 6. Same as Figure 3, but using the X-ray hot photon indices ($\Gamma_X^{\rm hot}$) and Eddington ratios ($R_{\rm Edd}^{\rm SED}$) of 34 NLSy1 and 30 BLSy1 galaxies based on the AGNSED model (Kubota & Done 2018) in the 0.3–10 keV energy band of the XMM-Newton data.

On the other hand, the significant $\Gamma_X^s - \log({\rm FWHM(H}\beta))$ anticorrelations are found for the samples of BLSy1 (with $\rho = -0.35$ and $P_{\rm null} = 9.91 \times 10^{-6}$) and [NLSy1+BLSy1] galaxies (with $\rho = -0.55$ and $P_{\rm null} = 2.87 \times 10^{-31}$). However, this correlation is found to be nominal for the sample of NLSy1s with $\rho = -0.21$ and $P_{\rm null} = 1.36 \times 10^{-3}$. A summary of all the above correlations, along with ρ and $P_{\rm null}$ values separately for the NLSy1s, BLSy1s, and their combined samples, is given in Table 5.

It may be noted here that the effect of soft X-ray excess, cold absorbers, warm absorbers, and other low-energy spectral complexities are generally prominent below 2 keV (Brandt et al. 1997) in the NLSy1 and BLSy1 galaxies. So, to confirm the aforementioned correlations, found for the samples of NLSy1 and BLSy1 galaxies between Γ_X^s and $\log(R_{\rm Edd})$, we analyzed the $\Gamma_X^h - \log(R_{\rm Edd})$ correlation in the hard energy (2–10 keV) band, which is thought to be probably less affected by soft X-ray excess. For this, we analyzed 53 NLSy1 and 46 BLSy1 galaxies for which Γ_X^h had been obtained (e.g., Section 4.2). The analysis of these two subsamples along with their joint subsample (i.e., [NLSy1+BLSy1]) resulted in a good positive correlation between Γ_X^h and $\log(R_{\rm Edd})$ for 53 NLSy1, 46 BLSy1, and 99 [NLSy1+BLSy1] galaxies with $\rho = 0.42$, 0.43, and 0.56, respectively. This can be seen in the top panels of Figure 8 and also from the middle part of Table 5. Mild anticorrelations are found between Γ_X^h and log(FWHM ($H\beta$)) for the subsamples of NLSy1, BLSy1, and [NLSy1 +BLSy1] galaxies with $\rho = -0.37$, -0.36, and -0.48, respectively. However, no significant correlations are found for $\Gamma_X^h - \log(L_{\rm bol})$ and $\Gamma_X^h - \log(M_{\rm BH})$ in these subsamples (see, e.g., Table 5 and Figure 8). The χ^2-minimization using the functional form of $y = mx + c$ (see above), with $y = \Gamma_X^h$ and X either $\log(R_{\rm Edd})$ or $\log({\rm FWHM}(H\beta))$, yielded for the subsample of NLSy1 galaxies as

$$\begin{aligned}\Gamma_X^h &= (0.29 \pm 0.06)\log(R_{\rm Edd}) + (2.33 \pm 0.03)\\ \Gamma_X^h &= (-0.70 \pm 0.13)\log({\rm FWHM}(H\beta)) + (4.35 \pm 0.41),\end{aligned} \tag{5}$$

for the subsample of BLSy1 galaxies as

$$\begin{aligned}\Gamma_X^h &= (0.17 \pm 0.09)\log(R_{\rm Edd}) + (2.03 \pm 0.14)\\ \Gamma_X^h &= (-0.26 \pm 0.20)\log({\rm FWHM}(H\beta)) + (2.71 \pm 0.73),\end{aligned} \tag{6}$$

and for the joint subsample of [NLSy1+BLSy1] galaxies as

$$\begin{aligned}\Gamma_X^h &= (0.35 \pm 0.03)\log(R_{\rm Edd}) + (2.34 \pm 0.03)\\ \Gamma_X^h &= (-0.68 \pm 0.06)\log({\rm FWHM}(H\beta)) + (4.27 \pm 0.19)\end{aligned} \tag{7}$$

as shown by solid red lines in the plots of Figure 8.

Additionally, the soft (0.1–2.0 keV) X-ray photon indices of most of the NLSy1s are affected by soft excess, and many of them also by absorption features due to "warm absorbers" (Vaughan et al. 1999). Therefore, a detailed X-ray spectral

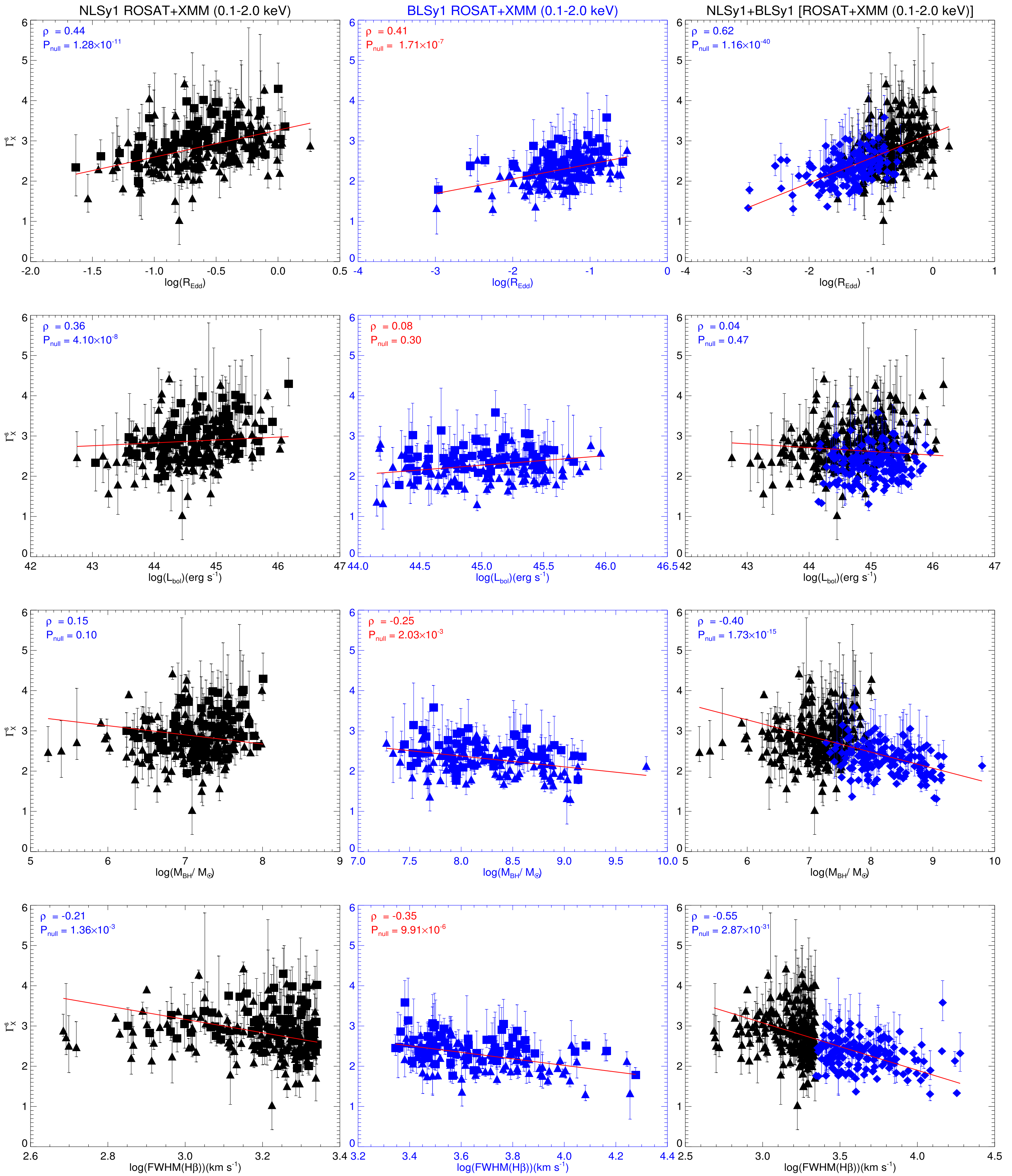

Figure 7. Correlations of the 221 NLSy1s (left) and 154 BLSy1s (middle) either from ROSAT (filled squares) or from XMM-Newton (filled triangles) for the soft (0.1–2.0 keV) X-ray photon indices (Γ_X^s) vs. Eddington ratios, bolometric luminosities, black hole masses, and FWHM of Hβ lines, respectively, from top to bottom panels, along with their error-weighted linear fit (red solid line). The last column presents the correlations among the same, but for the joint sample of 221 NLSy1s (black filled triangles) and 154 BLSy1s (blue filled diamonds). The plots also give the Spearman's correlation coefficient (ρ) and the probability of null correlation ($P_{\rm null}$) values (left corner of each panel).

Table 5

Results of the Correlation Analysis for the Samples of Soft X-Ray Energy Selected 221 NLSy1 and 154 BLSy1 Galaxies and the Subsamples of 53 NLSy1s, 46 BLSy1s and 139 NLSy1s, 97 BLSy1s of Hard and Total X-Ray Energies Selected, Respectively

ROSAT/XMM-Newton (0.1–2.0 keV)	NLSy1 (221 Sources)				BLSy1 (154 Sources)				NLSy1+BLSy1 (375 Sources)			
Correlation	m[a]	c[b]	ρ[c]	$P_{\rm null}$[d]	m[a]	c[b]	ρ[c]	$P_{\rm null}$[c]	m[a]	c[b]	ρ[c]	$P_{\rm null}$[b]
$\Gamma_X^s - \log(R_{\rm Edd})$	0.67 ± 0.04	3.27 ± 0.02	0.44	1.28×10^{-11}	0.37 ± 0.03	2.79 ± 0.04	0.41	1.71×10^{-7}	0.62 ± 0.02	3.19 ± 0.02	0.62	1.16×10^{-40}
$\Gamma_X^s - \log(L_{\rm bol})$	0.07 ± 0.02	-0.31 ± 0.88	0.36	4.10×10^{-8}	0.24 ± 0.04	-8.36 ± 1.56	0.08	0.30	-0.09 ± 0.02	6.81 ± 0.71	0.04	0.47
$\Gamma_X^s - \log(M_{\rm BH})$	-0.23 ± 0.02	4.50 ± 0.18	0.15	0.03	-0.27 ± 0.03	4.51 ± 0.28	−0.25	2.03×10^{-3}	-0.40 ± 0.01	5.68 ± 0.09	−0.40	1.73×10^{-15}
$\Gamma_X^s - \log(\text{FWHM}(H\beta))$	-1.66 ± 0.08	8.14 ± 0.27	−0.21	1.36×10^{-3}	-0.81 ± 0.07	5.27 ± 0.25	−0.35	9.91×10^{-6}	-1.18 ± 0.03	6.61 ± 0.10	−0.55	2.87×10^{-31}
XMM-Newton (2–10 keV)	NLSy1 (53 Sources)				BLSy1 (46 Sources)				NLSy1+BLSy1 (99 Sources)			
$\Gamma_X^h - \log(R_{\rm Edd})$	0.29 ± 0.06	2.33 ± 0.03	0.42	1.64×10^{-3}	0.17 ± 0.09	2.03 ± 0.14	0.43	2.65×10^{-3}	0.35 ± 0.03	2.34 ± 0.03	0.56	2.48×10^{-9}
$\Gamma_X^h - \log(L_{\rm bol})$	0.10 ± 0.07	-2.27 ± 2.99	0.23	0.10	0.11 ± 0.09	-3.23 ± 3.51	0.34	0.02	-0.06 ± 0.05	4.94 ± 2.15	0.09	0.38
$\Gamma_X^h - \log(M_{\rm BH})$	-0.27 ± 0.06	4.03 ± 0.43	−0.04	0.79	-0.02 ± 0.08	1.98 ± 0.65	−0.20	0.18	-0.28 ± 0.03	4.09 ± 0.19	−0.37	1.52×10^{-4}
$\Gamma_X^h - \log(\text{FWHM}(H\beta))$	-0.70 ± 0.13	4.35 ± 0.41	−0.37	6.47×10^{-3}	-0.26 ± 0.20	2.71 ± 0.73	−0.36	1.54×10^{-2}	-0.68 ± 0.06	4.27 ± 0.19	−0.48	3.57×10^{-7}
XMM-Newton (0.3–10 keV)	NLSy1 (139 Sources)				BLSy1 (97 Sources)				NLSy1+BLSy1 (236 Sources)			
$\Gamma_X^T - \log(R_{\rm Edd})$	0.51 ± 0.03	2.91 ± 0.03	0.42	3.84×10^{-7}	0.34 ± 0.02	2.56 ± 0.04	0.47	1.11×10^{-6}	0.50 ± 0.01	2.86 ± 0.02	0.56	2.76×10^{-21}
$\Gamma_X^T - \log(L_{\rm bol})$	0.06 ± 0.02	-0.18 ± 0.88	0.23	7.32×10^{-3}	0.02 ± 0.02	1.14 ± 1.05	0.14	0.17	-0.22 ± 0.01	12.23 ± 0.59	−0.03	0.68
$\Gamma_X^T - \log(M_{\rm BH})$	-0.22 ± 0.02	4.08 ± 0.18	−0.01	0.93	-0.28 ± 0.02	4.35 ± 0.17	−0.31	2.14×10^{-3}	-0.34 ± 0.01	4.91 ± 0.06	−0.41	9.05×10^{-11}
$\Gamma_X^T - \log(\text{FWHM}(H\beta))$	-1.32 ± 0.08	6.73 ± 0.25	−0.30	2.84×10^{-4}	-0.76 ± 0.05	4.87 ± 0.17	−0.41	2.62×10^{-5}	-0.91 ± 0.02	5.42 ± 0.07	−0.52	4.49×10^{-18}

Notes. The photon indices (in soft, hard, and total energy bands) are estimated using a simple power-law and absorption model.

[a], [b] Slope (m) and intercept (c) of a best-fit linear correlation of the form $y = mx + c$. In all the correlations $y = \Gamma_X$. The independent variables X are $X = \log(R_{\rm Edd})$ for the $\Gamma_X - \log(R_{\rm Edd})$ correlation, $X = \log(L_{\rm bol})$ for the $\Gamma_X - \log(L_{\rm bol})$ correlation, $X = \log(M_{\rm BH}/M_\odot)$ for the $\Gamma_X - \log(M_{\rm BH}/M_\odot)$ correlation, and $X = \log(\text{FWHM(H}\beta))$ for the $\Gamma_X - \log(\text{FWHM(H}\beta))$ correlation.

[c] Spearman's correlation coefficient (ρ).

[d] Probability of a null correlation from Spearman's test ($P_{\rm null}$).

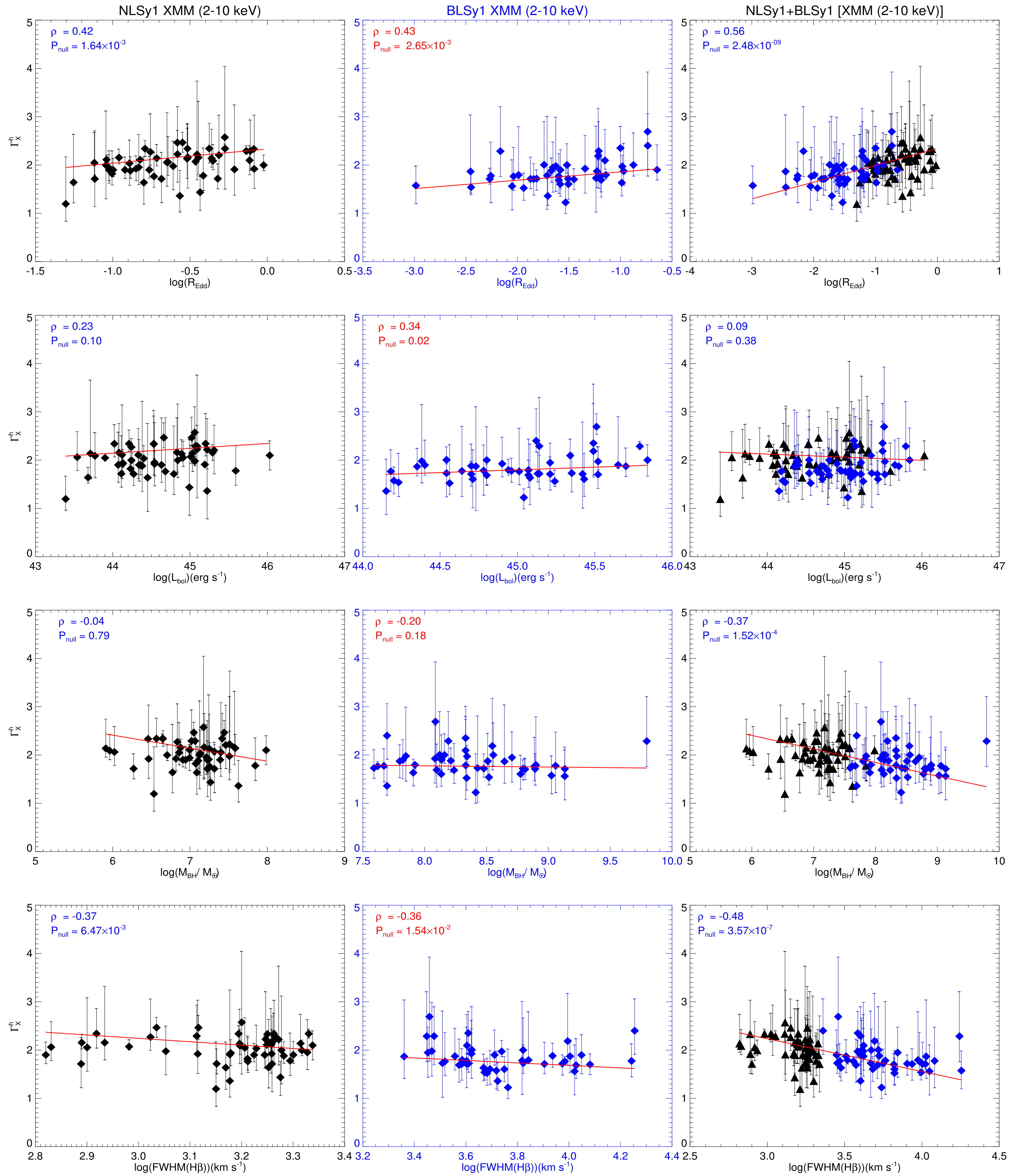

Figure 8. Same as Figure 7, but using the 53 NLSy1 and 46 BLSy1 galaxies for the XMM-Newton hard (2–10 keV) X-ray photon indices (Γ_X^h).

analysis in the 0.3–10 keV energy band is also carried out to confirm the aforementioned correlations found for the samples of NLSy1 and BLSy1 galaxies between Γ_X^s and $\log(R_{\rm Edd})$. For this, we analyzed 139 NLSy1 and 97 BLSy1 galaxies in the 0.3–10 keV energy band (e.g., Section 2) of XMM-Newton. The analysis of these two subsamples along with their joint subsample (i.e., [NLSy1+BLSy1]) resulted in a good positive correlation between Γ_X^T and $\log(R_{\rm Edd})$ for NLSy1, BLSy1, and

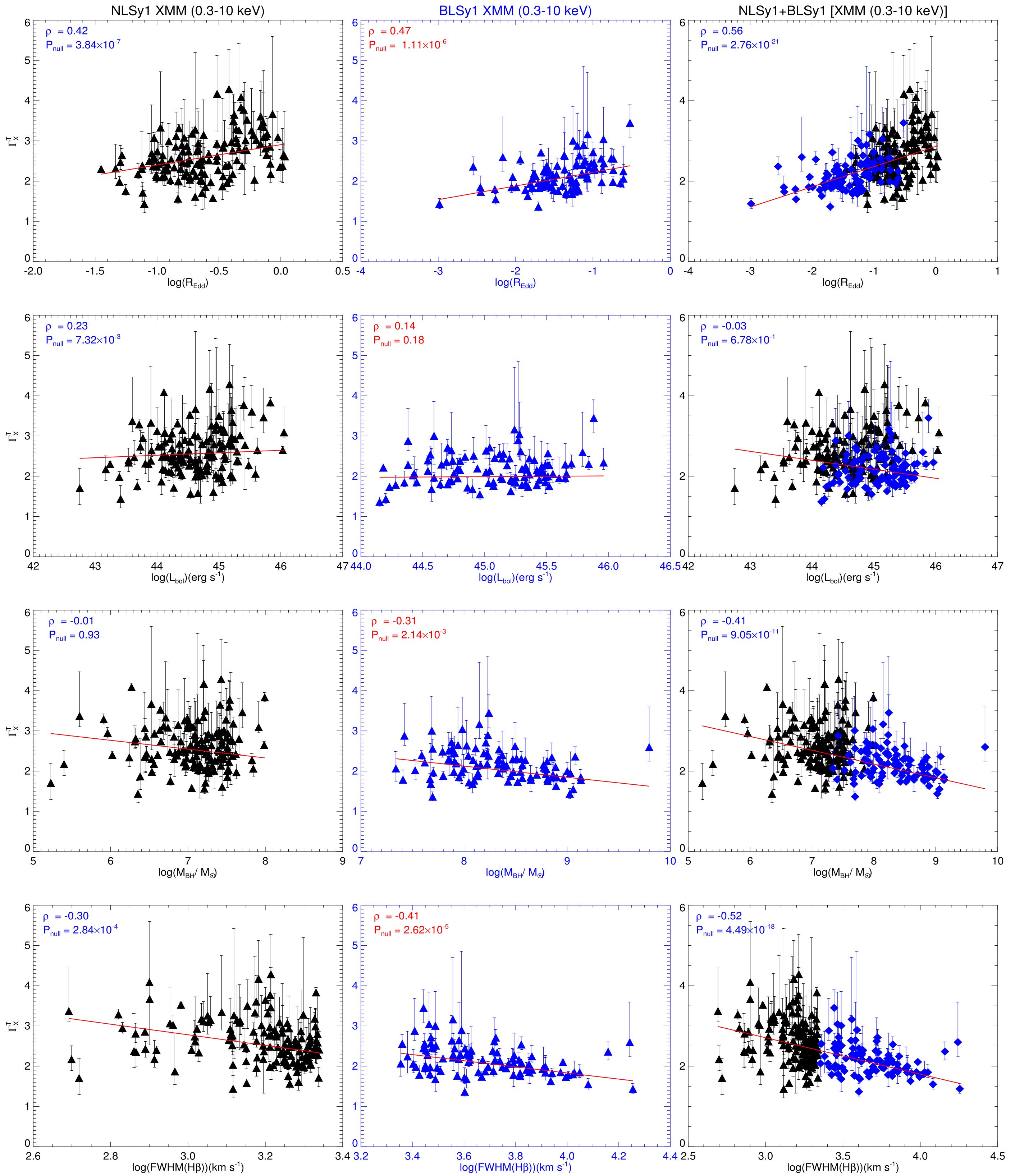

Figure 9. Same as Figure 7, but using the 139 NLSy1 and 97 BLSy1 galaxies for the XMM-Newton total (0.3–10 keV) X-ray photon indices (Γ_X^T).

[NLSy1+BLSy1] galaxies with $\rho = 0.42$, 0.47, and 0.56, respectively. This can be seen in the top panels of Figure 9 and also from the bottom part of Table 5. Mild anticorrelations are found between Γ_X^T and log(FWHM(Hβ)) for the subsamples of NLSy1s and BLSy1s with $\rho = -0.30$ and -0.41, respectively. This is found to be stronger with ρ of -0.52 when both subsamples are combined together. However, no significant correlations are found for $\Gamma_X^T - \log(L_{\rm bol})$ in these subsamples, except a mild anticorrelation found for $\Gamma_X^T - \log(M_{\rm BH})$ with ρ of −0.30 and −0.41, in the case of 97 BLSy1 and 236 [NLSy1+BLSy1] galaxies, respectively (see, e.g., Table 5 and Figure 9). The χ^2-minimization using the functional form of $y = mx + c$ (see above), with $y = \Gamma_X^T$ and X either $\log(R_{\rm Edd})$ or $\log(FWHM(H\beta))$, yielded for the subsample of NLSy1 galaxies as

$$\Gamma_X^T = (0.51 \pm 0.03)\log(R_{\rm Edd}) + (2.91 \pm 0.03)$$
$$\Gamma_X^T = (-1.32 \pm 0.08)\log(FWHM(H\beta)) + (6.73 \pm 0.25), \quad (8)$$

for the subsample of BLSy1 galaxies as

$$\Gamma_X^T = (0.34 \pm 0.02)\log(R_{\rm Edd}) + (2.56 \pm 0.04)$$
$$\Gamma_X^T = (-0.76 \pm 0.05)\log(FWHM(H\beta)) + (4.87 \pm 0.17), \quad (9)$$

and for the joint subsample of [NLSy1+BLSy1] galaxies as

$$\Gamma_X^T = (0.50 \pm 0.01)\log(R_{\rm Edd}) + (2.86 \pm 0.02)$$
$$\Gamma_X^T = (-0.91 \pm 0.02)\log(FWHM(H\beta)) + (5.42 \pm 0.07) \quad (10)$$

as shown by solid red lines in the plots of Figure 9.

Additionally, in view of the steeper Γ_X^s for the sample of NLSy1s and recalling that NLSy1 galaxies do have smaller FWHM of the emission lines as compared to BLSy1 galaxies, it will be worth exploring the possible correlation between FWHM of emission lines and X-ray spectral indices as well. Therefore, in the bottom panels of Figures 7–9, we have plotted Γ_X^s, Γ_X^h, and Γ_X^T versus log(FWHM(Hβ)) in the soft, hard, and total 0.3–10 keV energy bands, respectively. As can be seen from these figures (bottom right panel), the anticorrelation in Γ_X^s, Γ_X^h, and Γ_X^T versus log(FWHM(Hβ)) plots, based on the joint sample of NLSy1 and BLSy1 galaxies, is significant with $\rho = -0.55$, −0.48, and −0.52, with their corresponding $P_{\rm null}$ of 2.87×10^{-31}, 3.57×10^{-7}, and 4.49×10^{-18}, respectively (see Table 5).

5.3. Comparison of the $\Gamma_X^{\rm hot}$ Correlations with AGN Parameters among the Subsamples of NLSy1 and BLSy1 Galaxies

As detailed in Section 4.4, we could achieve a spectral fit in the 0.3–10 keV energy band for 34 NLSy1 and 30 BLSy1 galaxies, based on the AGNSED model. This allowed us to estimate the hot spectral indices ($\Gamma_X^{\rm hot}$) for these sources, along with their correlations with $R_{\rm Edd}^{\rm SED}$, $L_{\rm bol}$, $M_{\rm BH}$, and FWHM(Hβ). The plots of these correlation analyses are shown in Figure 10, and the results are listed in the upper part of Table 6. From this table and the figure, it is clear that the correlations of $\Gamma_X^{\rm hot}$ with other parameters of nuclear activities are almost similar to those obtained in the 0.1–2.0 keV energy band for the NLSy1 (221 sources), BLSy1 (154 sources), and [NLSy1+BLSy1] (375 sources) galaxies.

6. Discussion and Conclusions

In order to probe the X-ray emission mechanisms in NLSy1 and BLSy1 galaxies, a correlation study among X-ray spectral indices and parameters of nuclear activity such as $R_{\rm Edd}$, $L_{\rm bol}$, $M_{\rm BH}$, and FWHM(Hβ) would be very important. For instance, Brandt et al. (1997) analyzed an Advanced Satellite for Cosmology and Astrophysics (ASCA) sample of 15 NLSy1 and 19 BLSy1 galaxies, for the comparison of their hard X-ray (2–10 keV) photon indices, and found that NLSy1s have steeper intrinsic hard X-ray photon indices than the BLSy1s. Here we have extended similar work by studying the soft (0.1–2.0 keV), hard (2–10 keV), and total (0.3–10 keV) photon indices (i.e., Γ_X^s, Γ_X^h, and Γ_X^T) of NLSy1 and BLSy1 galaxies. For this, we have constructed their samples based on the recent large catalog of 11,101 NLSy1s and their redshift-matched sample of BLSy1s using their X-ray data from ROSAT and XMM-Newton (e.g., Section 2). Our sample consists of 221 NLSy1 and 154 BLSy1 galaxies in the soft energy band (0.1–2.0 keV), 53 NLSy1 and 46 BLSy1 galaxies in the hard energy band (2–10 keV), and 139 NLSy1 and 97 BLSy1 galaxies in the total energy band (0.3–10 keV) (e.g., Section 2). A homogeneous analysis is carried out for the estimations of Γ_X^s, Γ_X^h, Γ_X^T, and other parameters of nuclear activities, such as $R_{\rm Edd}$, $L_{\rm bol}$, $M_{\rm BH}$, and FWHM(Hβ) of the NLSy1 and BLSy1 galaxies. This homogeneous analysis is carried out to perform a comparative study between these two subclasses of AGNs, along with a comparison of them with other classes of luminous AGNs in soft, hard, and total X-ray energy bands.

The advantages of our analysis are that we have used an enlarged sample of NLSy1s (see, e.g., Table 1). For comparison, we have used a control sample of BLSy1s, matching (moderately) in the redshift plane (see, e.g., Figure 1 and Section 2). Furthermore, in our analysis, to compute the soft, hard, and total energy X-ray photon indices, we have used similar models (mostly) in the soft, hard, and total energy X-ray bands. This extra caution is taken in our method so as to avoid the variations in the estimated Γ_X^s, Γ_X^h, and Γ_X^T due to the use of different spectral fitting models, as has been the case in many previous studies as mentioned in Section 1.

The main results of our systematic homogeneous analysis presented here are as follows. First, we found a clear significant difference among the Γ_X^s distribution of NLSy1 and BLSy1 galaxies (being steeper for the NLSy1 class; see, e.g., Figure 3), with median values of 2.81 and 2.30 for the samples of the NLSy1 and BLSy1 galaxies, respectively, having $P_{\rm null}$ of 4.02×10^{-19} based on the K-S test. One reason for this observed difference among the Γ_X^s distribution of NLSy1 and BLSy1 galaxies could be more soft X-ray excess in NLSy1s. To lift this degeneracy, we have compared Γ_X^h, which are thought to be free from the soft X-ray excess (see, e.g., Boller et al. 1996; Brandt et al. 1997; Vaughan et al. 1999; Boller et al. 2002; Czerny et al. 2003; Vignali et al. 2004), between the subsamples of 53 NLSy1 and 46 BLSy1 galaxies based on their 2–10 keV XMM-Newton observations. In this comparison also we find a difference in Γ_X^h with median values of 2.06 and 1.78, having $P_{\rm null}$ of 1.00×10^{-3} for the subsamples of NLSy1 and BLSy1 galaxies, respectively (see, e.g., Figure 4). This confirms that the above result of the difference in Γ_X^s distribution is unlikely to be solely due to the soft X-ray excess and rather seems to be intrinsic in their nature. Furthermore, we noticed that the difference in the median photon indices of hard energy band subsamples of NLSy1 and BLSy1 galaxies is statistically weaker than the soft energy band samples of NLSy1 and BLSy1 galaxies. This may be due to comparatively about 4 times smaller hard-band subsamples of NLSy1 and BLSy1 galaxies. To lift this degeneracy, we have compared the Γ_X^T between the subsamples of 139 NLSy1 and 97 BLSy1 galaxies. We again find a significant difference with

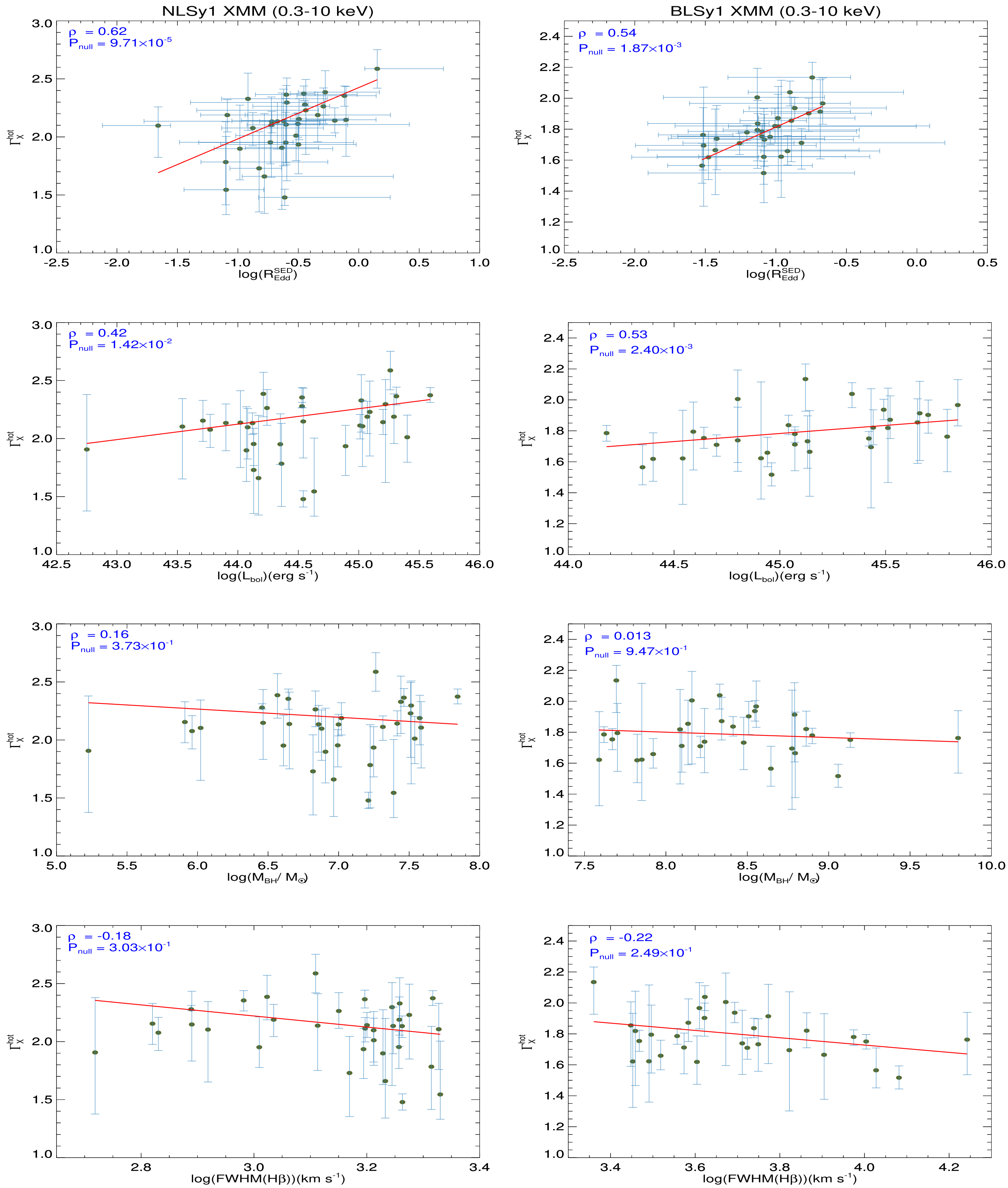

Figure 10. Same as Figure 7, but using the spectral fit of 34 NLSy1 and 30 BLSy1 galaxies based on the AGNSED model for the X-ray hot photon indices ($\Gamma_X^{\rm hot}$) in the 0.3–10 keV energy band of the XMM-Newton data.

median values of 2.53 and 2.13, respectively, having $P_{\rm null}$ of 4.50×10^{-9}, which is consistent with the result based on soft X-ray analysis of these NLSy1 and BLSy1 galaxies.

Second, to ascertain whether there is a bimodality or continuity in X-ray spectral indices (hereafter Γ_X will be referred to as Γ_X^s, Γ_X^h, and Γ_X^T) among NLSy1 and BLSy1 galaxies. A detailed correlation analysis of Γ_X with other physical parameters of AGNs such as $R_{\rm Edd}$, $L_{\rm bol}$, $M_{\rm BH}$, and FWHM(Hβ) is carried out. This correlation analysis results in the strongest $\Gamma_X - \log(R_{\rm Edd})$ correlation for the samples of NLSy1 and BLSy1 galaxies (e.g., Section 5.2 and Table 5), implying that $R_{\rm Edd}$ may be the dominant parameter related to Γ_X. Additionally, the joint analysis of [NLSy1+BLSy1] shows that the variation seems to be continuous rather than a clear

Table 6
Results of the Correlation Analysis in 0.3–10 keV for the Samples of 34 NLSy1 and 30 BLSy1 Galaxies Using the AGNSED Model

XMM-Newton (0.3–10.0 keV) Correlation[a]	NLSy1 (34 Sources)				BLSy1 (30 Sources)			
	m	c	ρ	$P_{\rm null}$	m	c	ρ	$P_{\rm null}$
$\Gamma_X^{\rm hot} - \log(R_{\rm Edd}^{\rm SED})$	0.44 ± 0.09	2.42 ± 0.04	0.62	9.71×10^{-5}	0.40 ± 0.11	2.22 ± 0.11	0.54	1.87×10^{-3}
$\Gamma_X^{\rm hot} - \log(L_{\rm bol})$	0.13 ± 0.04	−3.74 ± 1.83	0.42	1.42×10^{-2}	0.10 ± 0.04	−2.92 ± 1.77	0.53	2.40×10^{-3}
$\Gamma_X^{\rm hot} - \log(M_{\rm BH})$	−0.07 ± 0.03	2.69 ± 0.24	0.16	3.73×10^{-1}	0.04 ± 0.03	−2.08 ± 0.28	0.01	9.47×10^{-1}
$\Gamma_X^{\rm hot} - \log(FWHM\,(H\beta))$	−0.48 ± 0.10	3.65 ± 0.30	−0.18	3.03×10^{-1}	−0.24 ± 0.08	2.67 ± 0.32	−0.22	2.49×10^{-1}
$\log(R_{\rm Edd}^{\rm SED}) - \log(R_{\rm Edd})$	0.30 ± 0.10	−0.42 ± 0.02	0.47	2.44×10^{-3}	0.14 ± 0.12	−0.82 ± 0.20	0.51	7.28×10^{-4}

Note.
[a] The correlation parameters are the same as Table 5, but in $y = mx + c$ fit, for $y = \Gamma_X^{\rm hot}$ in all the correlations and $X = \log(R_{\rm Edd}^{\rm SED})$ in the $\Gamma_X^{\rm hot} - \log(R_{\rm Edd}^{\rm SED})$ correlation. In the last row y and x are $\log(R_{\rm Edd}^{\rm SED})$ and $\log(R_{\rm Edd})$, respectively.

significant bimodality in its distribution (see, e.g., last column of Figures 7–9). This is also evident in their joint histogram plots of Γ_X, which do not show two well-separated significant peaks (see, e.g., histogram of joint [NLSy1+BLSy1] distribution in Figures 3–5). Furthermore, the similarity of the trends and value of Spearman's correlations for the $\Gamma_X - \log(R_{\rm Edd})$ correlation found for NLSy1 and BLSy1 galaxies in the soft, hard, and total X-ray energy bands (see, e.g., Table 5) also suggest that their emission mechanism may be similar. However, the slopes of the linear fit of Γ_X and $\log(R_{\rm Edd})$ correlations do differ significantly among the samples of NLSy1 and BLSy1 galaxies in soft, hard, and total X-ray energy bands (see, e.g., Table 5), which could probably be due to the difference in their accretion rates, being higher for the former.

We explored this possibility by comparing the distribution of $R_{\rm Edd}$ of NLSy1 and BLSy1 galaxies. This has resulted in the median values of $R_{\rm Edd}$, 0.23 and 0.05 for 221 NLSy1 and 154 BLSy1 galaxies, respectively, in the soft X-ray. The $R_{\rm Edd}$ distribution differs significantly for the above samples of NLSy1 and BLSy1 galaxies with a K-S test based $P_{\rm null} = 2.66 \times 10^{-35}$. The above result also holds when we compare in the 0.3–10 keV energy band. The distributions of $R_{\rm Edd}$ of 139 NLSy1 and 97 BLSy1 galaxies have median values of 0.22 and 0.04, respectively, with a K-S test based $P_{\rm null}$ of 3.72×10^{-26}. Similarly, using the analysis of 53 NLSy1 and 46 BLSy1 galaxies in the hard energy band, the median values of $R_{\rm Edd}$ are found to be 0.25 and 0.03, respectively, resulting in a K-S test based $P_{\rm null}$ of 1.72×10^{-14}. In view of the above, negligible dependence of the $P_{\rm null}$ values on the energy bands used in the analysis allows us to conclude that the $R_{\rm Edd}$ of NLSy1 and BLSy1 galaxies seem to be intrinsically significantly different, being higher for the former.

To reconcile this discrepancy, one possibility is that the higher $R_{\rm Edd}$ in NLSy1s (compared to BLSy1s) can be due to the fact that the inclination angle of the NLSy1 is lower than that of the BLSy1. As a result, the observed FWHM (in km s^{-1}) of the Hβ line (FWHM × sin(θ)) of the broad-line region (BLR) would have been underestimated more in the case of NLSy1 (due to smaller inclination) compared to the BLSy1 (see, e.g., Baldi et al. 2016; Liu et al. 2016; Rakshit et al. 2017). This will directly impact the underestimation of their $M_{\rm BH}$ (being proportional to the observed FWHM in the common L–$R_{\rm BLR}$ scaling relationship) and hence the overestimation of the $R_{\rm Edd}$ value (being inversely proportional to $M_{\rm BH}$). To consider such a projection effect of the BLR for the NLSy1 and BLSy1 galaxies in our analysis, we corrected the observed FWHM (i.e., projected) values as FWHM/sin(θ), by using the median viewing angle (θ) of 13°.6 and 27°.7 as given by Liu et al. (2016) for the NLSy1s and BLSy1s, respectively. This has allowed us to have corrected $M_{\rm BH}$ and $R_{\rm Edd}$ for our samples of NLSy1 and BLSy1 galaxies. The corrected $R_{\rm Edd}$ values still show a difference (though with less statistical significance) among its distribution in 221 NLSy1 and 154 BLSy1 galaxies with a K-S test based $P_{\rm null} = 3.45 \times 10^{-2}$. The difference still exists when we even use only the subsamples of 139 NLSy1 and 97 BLSy1 galaxies analyzed in the 0.3–10 keV energy range, giving $P_{\rm null} = 2.18 \times 10^{-2}$. Here, a possibility also exists that it may also be due to the imperfection of exact luminosities matching and/or due to our application of the average inclination angle value for the entire sample. Nonetheless, the fact that the mismatch in luminosities in our sample is nominal and the fact that the $R_{\rm Edd}$ difference is very significant suggest that it is intrinsically higher in NLSy1 compared to BLSy1. This could lead to the above-measured differences in Γ_X^s, Γ_X^h, Γ_X^T distributions and the slopes of the linear fit of the Γ_X and $\log(R_{\rm Edd})$ correlations.

Another possibility for the above difference in the $R_{\rm Edd}$ can be due to under/overestimations of bolometric luminosity, which was estimated using the scaling relationship of $L_{\rm bol}$ and optical luminosity at 5100 Å (e.g., Section 4.2). To quantify its effect, we have also estimated the $R_{\rm Edd}$ values independently by fitting the AGNSED model over the 0.3–10 keV band (i.e., $R_{\rm Edd}^{\rm SED}$) for the 34 NLSy1 and 30 BLSy1 galaxy subsamples (e.g., Section 4.4). The resulting distribution of $R_{\rm Edd}^{\rm SED}$ (see, e.g., Figure 6) has also shown a significant difference (with $P_{\rm null} = 2.01 \times 10^{-7}$) in the subsamples of these 34 NLSy1 and 30 BLSy1 galaxies. This is consistent with the conclusion drawn using the $R_{\rm Edd}$ distribution, based on $L_{\rm bol}$ estimated using the optical spectra (see, e.g., Figures 3–5). This is not surprising because there is a significant correlation between $R_{\rm Edd}$ (i.e., using optical) and $R_{\rm Edd}^{\rm SED}$ (i.e., using X-ray) for the NLSy1 and BLSy1 galaxies as shown in Figure 11 and tabulated in the last row of Table 6. Furthermore, the histograms of spectral indices estimated using the AGNSED model ($\Gamma_X^{\rm SED}$, also presented as $\Gamma_X^{\rm hot}$ in Figure 10) also show a significant difference among NLSy1 and BLSy1 galaxies with $P_{\rm null}$ of 8.87×10^{-6} (see, e.g., Figure 6). In addition to this, a correlation between $\Gamma_X^{\rm hot}$ and $\log(R_{\rm Edd}^{\rm SED})$ is also found in the above subsamples of NLSy1 and BLSy1 galaxies (see, e.g., Figure 10), which is similar to the correlations found in the soft, hard, and total energy bands between Γ_X and $R_{\rm Edd}$.

Our above investigations suggest that the $R_{\rm Edd}$ of NLSy1 galaxies is unambiguously higher than that of BLSy1 galaxies.

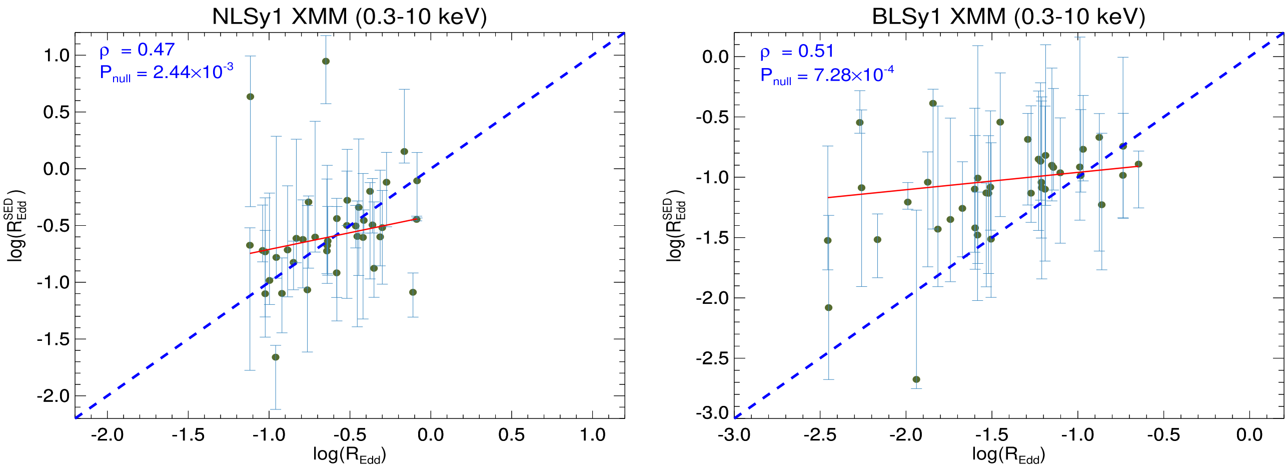

Figure 11. Correlations of 34 NLSy1s (left) and 30 BLSy1s (right) for the X-ray Eddington ratio ($\log(R_{\rm Edd}^{\rm SED})$) and optical Eddington ratio ($\log(R_{\rm Edd})$) obtained from X-ray fitting in the 0.3–10 keV energy band using the AGNSED model and optical scaling relationship (see Section 4.1), respectively. The dotted blue line is plotted in each panel following the equation $y = x$.

This intrinsic difference can explain our observed significant difference of spectral indices among NLSy1 and BLSy1 galaxies as follows.

The higher value of $R_{\rm Edd}$ can lead to an increase in the disk temperature, hence producing more X-ray radiations, and at the same time, it can also increase the Compton cooling of corona (Haardt & Maraschi 1991, 1993; Zdziarski et al. 2000; Kawaguchi et al. 2001), which leads to steepening of the X-ray power law more in NLSy1 than in BLSy1, and hence will lead to the observed difference we noticed in our spectral indices in the soft, hard, and total 0.3–10 keV energy bands (e.g., Section 5.1). Moreover, this also could be the reason for the observed higher slope of Γ_X and $\log(R_{\rm Edd})$ linear fit for NLSy1 galaxies compared to BLSy1 galaxies (see, e.g., Table 5), as such a stronger dependence in the case of NLSy1 galaxies can be reconciled owing to their higher $R_{\rm Edd}$ value.

As pointed out in Section 1, such a positive $\Gamma_X^h - \log(R_{\rm Edd})$ correlation (see, e.g., Table 5) has also been found for the luminous AGNs by Risaliti et al. (2009). It may be noted that they found a ρ of 0.32 based on their sample of 343 AGNs. However, this correlation becomes stronger with the value of $\rho = 0.56$ when considering only their subset of 82 objects whose black hole masses were estimated using their Hβ lines. This is almost similar to the Spearman's correlation coefficients found for the $\Gamma_X^s - \log(R_{\rm Edd})$, $\Gamma_X^h - \log(R_{\rm Edd})$, and $\Gamma_X^T - \log(R_{\rm Edd})$ correlations in our samples of the NLSy1 and BLSy1 galaxies (see, e.g., Table 5). On the other hand, the striking contrast to this positive correlation as compared to the corresponding negative correlation found for the case of LLAGNs by Gu & Cao (2009) suggests that the emission mechanism in the NLSy1 and BLSy1 galaxies is different as compared to the LLAGNs but likely to be similar to the luminous AGNs.

Finally, we have also explored the correlation of X-ray spectral slopes (in the soft energy band) with that of the optical plane of Eigenvector 1 (EV1), which is mainly defined by FWHM(Hβ) and the flux ratio of Fe II to Hβ, $R_{\rm FeII}$ (Sulentic et al. 2000). The FWHM(Hβ) is known to be affected by the inclination angle, while the $R_{\rm FeII}$ is driven by the Eddington ratio (Shen & Ho 2014). The $R_{\rm FeII}$ values of NLSy1 galaxies are taken from the parent catalog of NLSy1 galaxies given by Rakshit et al. (2017), and for the BLSy1 galaxies, it is

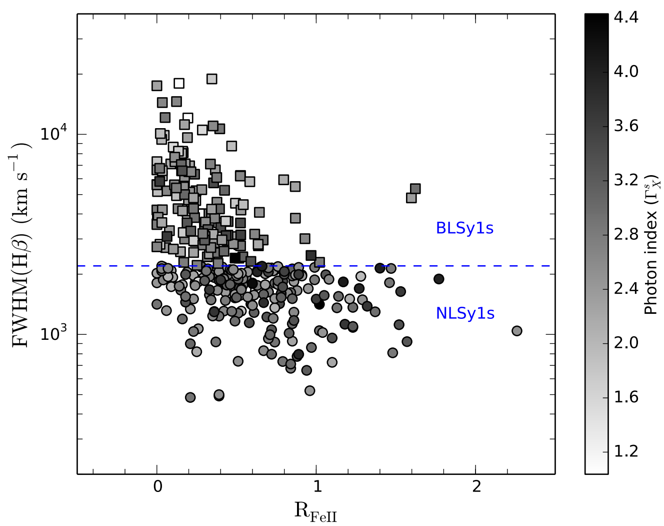

Figure 12. Plot of Eigenvector 1 EV1 ($R_{\rm Fe\,II}$ vs. FWHM(H(β))) with space gray coded by the soft (0.1–2.0 keV) X-ray photon indices (Γ_X^s) for the 221 NLSy1 (gray filled circle) and 154 BLSy1 (gray filled square) galaxies.

estimated following a similar procedure to that used in Rakshit et al. (2017) for the NLSy1 galaxies. In Figure 12, we have plotted these quantities color-coded by the Γ_X^s. We find strong Fe II emitters to have steeper photon indices compared to the weak Fe II emitters. The Spearman's rank correlation coefficients between $R_{\rm FeII}$ and Γ_X^s are found to be 0.31 and 0.24 for the samples of NLSy1 and BLSy1 galaxies, respectively, while it is 0.46 when both NLSy1 and BLSy1 samples are combined together. This positive correlation between Γ_X^s and $R_{\rm FeII}$ reflects the strong correlation found between photon indices and Eddington ratios. Moreover, Figure 12 also corroborates the strong anticorrelation between photon indices and FWHM(Hβ) found in the joint analysis of NLSy1 and BLSy1 samples (e.g., Section 5.2 and Figures 7–9). In view of such a strong anticorrelation, we may recall that Γ_X being related to the X-ray-emitting regions is generally much closer to the central engine of AGNs as compared to BLR clouds, whose broadening is measured as the FWHM of Hβ lines. As a result, such a strong anticorrelation between these two seemingly disconnected regions is worth noting while constructing any models of the AGN emission mechanisms along with the observed strong correlation of the $\Gamma_X - \log(R_{\rm Edd})$ found for both NLSy1 and BLSy1 galaxies.

7. Summary

In this work, we have quantitatively compared NLSy1 and BLSy1 galaxies for their X-ray and optical properties, along with different correlations among X-ray and optical parameters, such as $\Gamma_X - \log(R_{\rm Edd})$, $\Gamma_X - \log(L_{bol})$, $\Gamma_X - \log(M_{\rm BH})$, and $\Gamma_X - \log(FWHM(H\beta))$, with Γ_X representing X-ray spectral slope in soft (i.e., Γ_X^s in 0.1–2.0 keV), hard (i.e., Γ_X^h in 2–10 keV), and total (0.3–10 keV) energy bands (i.e., Γ_X^T). For these, we used the samples of 221 NLSy1 and 154 BLSy1 galaxies in the soft X-ray energy (0.1–2.0 keV) band, while its subsamples of 53 NLSy1 and 46 BLSy1 galaxies and 139 NLSy1 and 97 BLSy1 galaxies are used also in the hard X-ray and total energy bands, respectively. The summary of our main results is as follows:

(i) We found the existence of difference in Γ_X^s distribution among the NLSy1 and BLSy1 galaxies, being steeper for the former in the soft X-ray energy band. Furthermore, the difference is also found when spectral indices of these two subsets are compared in hard and total energy bands (i.e., Γ_X^h and Γ_X^T). In view of the fact that the hard energy band is generally less prone to the impact of soft X-ray excess, it suggests that soft X-ray excess is not the main cause of the difference seen here among the Γ_X found for the NLSy1 and BLSy1 galaxies.

(ii) We found a clear significant difference in $R_{\rm Edd}$ among NLSy1 and BLSy1 galaxies, being larger for the former with $P_{\rm null}$ of 2.66×10^{-35}. This difference exists even after incorporating any inclination angle difference among these two subclasses, though with less significance. Furthermore, this discrepancy (based on $R_{\rm Edd}$ from the optical data) is also reconfirmed even when we estimated $R_{\rm Edd}$ independently based on SED fitting (AGNSED model) in the X-ray 0.3–10 keV band (e.g., Section 4.4). This suggests that $R_{\rm Edd}$ of the NLSy1 is intrinsically higher than the BLSy1 galaxy, which can be the main reason for the observed significant difference in Γ_X among NLSy1 and BLSy1 galaxies in soft, hard, and total energy bands.

(iii) Our analysis suggests a significant positive correlation between Γ_X and $\log(R_{\rm Edd})$ for the samples of NLSy1 and BLSy1 galaxies in soft, hard, and total energy bands, with stronger dependence in the case of NLSy1s. Also, these strong correlations between Γ_X and $\log(R_{\rm Edd})$ for the NLSy1 and BLSy1 galaxies show that their X-ray slope can be used as an Eddington ratio estimator, which can then also be used to calculate black hole mass for a given bolometric luminosity estimate.

(iv) Overall correlations such as $\Gamma_X - \log(R_{\rm Edd})$ have almost similar trends among the NLSy1 and BLSy1 galaxies. These correlations are found to be also consistent (qualitatively) with the luminous AGNs (at least in hard X-ray), apart from their higher significance compared to NLSy1 and BLSy1 galaxies. This gives support to the theoretical prediction that the X-ray emissions may also be produced in NLSy1 and BLSy1 galaxies by the disk-corona system as proposed for the case of luminous AGNs. This model is also consistent with the steeper Γ_X we have found in our samples of NLSy1 galaxies in comparison to the BLSy1 galaxies.

We thank the anonymous referee for the constructive comments on our manuscript. We gratefully acknowledge Mainpal Ranjan, Jeewan C. Pandey, and Xinwu Cao for their very useful discussions.

ORCID iDs

Vineet Ojha https://orcid.org/0000-0001-5878-4811
Gulab Chand Dewangan https://orcid.org/0000-0003-1589-2075
Suvendu Rakshit https://orcid.org/0000-0002-8377-9667

References

Alam, S., Albareti, F. D., Allende Prieto, C., et al. 2015, ApJS, 219, 12
Arnaud, K. A. 1996, in ASP Conf. Ser. 101, Astronomical Data Analysis Software and Systems V, ed. G. H. Jacoby & J. Barnes (San Francisco, CA: ASP), 17
Baldi, R. D., Capetti, A., Robinson, A., Laor, A., & Behar, E. 2016, MNRAS, 458, L69
Bennett, C. L., Larson, D., Weiland, J. L., & Hinshaw, G. 2014, ApJ, 794, 135
Boller, T., Brandt, W. N., & Fink, H. 1996, A&A, 305, 53
Boller, T., Fabian, A. C., Sunyaev, R., et al. 2002, MNRAS, 329, L1
Boller, T., Freyberg, M. J., Trümper, J., et al. 2016, A&A, 588, A103
Boroson, T. A. 2002, ApJ, 565, 78
Boroson, T. A., & Green, R. F. 1992, ApJS, 80, 109
Brandt, W. N., Mathur, S., & Elvis, M. 1997, MNRAS, 285, L25
Collin, S., & Kawaguchi, T. 2004, A&A, 426, 797
Czerny, B., Nikołajuk, M., Różańska, A., et al. 2003, A&A, 412, 317
Dickey, J. M., & Lockman, F. J. 1990, ARA&A, 28, 215
Dorman, B., & Arnaud, K. A. 2001, in ASP Conf. Ser. 238, Astronomical Data Analysis Software and Systems X, ed. F. R. Harnden, Jr., F. A. Primini, & H. E. Payne (San Francisco, CA: ASP), 415
Esin, A. A., McClintock, J. E., & Narayan, R. 1997, ApJ, 489, 865
Gayathri, V., Bacon, P., Pai, A., et al. 2019, PhRvD, 100, 124022
González-Martín, O., Masegosa, J., Márquez, I., Guerrero, M. A., & Dultzin-Hacyan, D. 2006, A&A, 460, 45
Grupe, D., Beuermann, K., Mannheim, K., & Thomas, H.-C. 1999, A&A, 350, 805
Grupe, D., Beuermann, K., Thomas, H.-C., Mannheim, K., & Fink, H. H. 1998, A&A, 330, 25
Gu, M., & Cao, X. 2009, MNRAS, 399, 349
Haardt, F., & Maraschi, L. 1991, ApJ, 380, L51
Haardt, F., & Maraschi, L. 1993, ApJ, 413, 507
Kawaguchi, T., Shimura, T., & Mineshige, S. 2001, ApJ, 546, 966
Klimek, E. S., Gaskell, C. M., & Hedrick, C. H. 2004, ApJ, 609, 69
Komossa, S., & Meerschweinchen, J. 2000, A&A, 354, 411
Kshama, S. K., Paliya, V. S., & Stalin, C. S. 2017, MNRAS, 466, 2679
Kubota, A., & Done, C. 2018, MNRAS, 480, 1247
Laor, A., Fiore, F., Elvis, M., Wilkes, B. J., & McDowell, J. C. 1997, ApJ, 477, 93
Leighly, K. M. 1999, ApJS, 125, 297
Liu, X., Yang, P., Supriyanto, R., & Zhang, Z. 2016, IJAA, 6, 166
Lu, Y., & Yu, Q. 1999, ApJ, 526, L5
Maoz, D. 2007, MNRAS, 377, 1696
McLure, R. J., & Dunlop, J. S. 2004, MNRAS, 352, 1390
Miller, H. R., Ferrara, E. C., McFarland, J. P., et al. 2000, NewAR, 44, 539
Ojha, V., Chand, H., Krishna, G., Mishra, S., & Chand, K. 2020, MNRAS, 493, 3642
Ojha, V., Krishna, G., & Chand, H. 2019, MNRAS, 483, 3036
Osterbrock, D. E., & Pogge, R. W. 1985, ApJ, 297, 166
Paliya, V. S., Sahayanathan, S., Parker, M. L., et al. 2014, ApJ, 789, 143
Panessa, F., Bassani, L., Cappi, M., et al. 2006, A&A, 455, 173
Pounds, K. A., Done, C., & Osborne, J. P. 1995, MNRAS, 277, L5
Pounds, K. A., Nandra, K., Fink, H. H., & Makino, F. 1994, MNRAS, 267, 193
Rakshit, S., & Stalin, C. S. 2017, ApJ, 842, 96
Rakshit, S., Stalin, C. S., Chand, H., & Zhang, X.-G. 2017, ApJS, 229, 39
Risaliti, G., Young, M., & Elvis, M. 2009, ApJ, 700, L6
Schneider, D. P., Hall, P. B., Richards, G. T., et al. 2005, AJ, 130, 367
Shen, Y., & Ho, L. C. 2014, Natur, 513, 210

Shuder, J. M., & Osterbrock, D. E. 1981, ApJ, 250, 55
Sulentic, J. W., Zwitter, T., Marziani, P., & Dultzin-Hacyan, D. 2000, ApJ, 536, L5
Vaughan, S., Reeves, J., Warwick, R., & Edelson, R. 1999, MNRAS, 309, 113
Vestergaard, M., & Peterson, B. M. 2006, ApJ, 641, 689
Vignali, C., Brandt, W. N., Boller, T., Fabian, A. C., & Vaughan, S. 2004, MNRAS, 347, 854
Wandel, A., Milgrom, M., & Yahil, A. 1985, ApJ, 292, 206
Wang, T., Brinkmann, W., & Bergeron, J. 1996, A&A, 309, 81
Zdziarski, A. A., Poutanen, J., & Johnson, W. N. 2000, ApJ, 542, 703
Zhou, H., Wang, T., Yuan, W., et al. 2006, ApJS, 166, 128